Réunions AstroDoc

Le travail de l'équipe DJIN
07/12/2017

CENTRE DE DONNÉES
ASTRONOMIQUES DE STRASBOURG

Equipe DJIN

Les journaux indexés

Priorité 1

A&A Astronomy & Astrophysics
AJ Astronomical Journal
ApJ AstroPhysical Journal
ApJS AstroPhysical Journal Supplement Series
MNRAS Monthly Notices of the Royal Astronomical Society
Natur Nature
PASJ Publication of the Astronomical Society of Japan
PASP Publication of the Astronomical Society of the Pacific
Sci Science

Les journaux indexés

	Références par an (2016)
A&A	1852
AJ	388
ApJ	3758
ApJS	183
MNRAS	3258
Natur	40
PASJ	123
PASP	94
Sci	12

Total : 9708 références en 2016

Les journaux indexés

Priorité 2

Aca	Acta Astronomica
Raa	Research in Astronomy and Astrophysic
Atel	Astronomers Telegram
GCN	Gamma-ray Burst Coordinates Network
NewA	New Astronomy

Les journaux indexés

Priorité 2

	Références par année (2016)
Aca	16 (2015)
Raa	103
Atel	1626 (2015)
GCN	1500
NewA	69

Total : 3314 références

Les journaux indexés

Total : 13022 références par an

Soit 18 articles par jour

MISSION DE BASE

Attacher les objets aux références de la littérature scientifique

MISSION DE BASE

Attacher les objets aux références de la littérature scientifique

Créer les références bibliographiques le cas échéant

MISSION DE BASE

Attacher les objets aux références de la littérature scientifique

Créer les références bibliographiques le cas échéant

Dispatcher les références aux autres équipes (Dictionnaire, VizieR, Cosim) et aux astronomes pour expertise scientifique et mise à jour des données fondamentales

MISSION DE BASE

Attacher les objets aux références de la littérature scientifique

Créer les références bibliographiques le cas échéant

Dispatcher les références aux autres équipes (Dictionnaire, VizieR, Cosim) et aux astronomes pour expertise scientifique et mise à jour des données fondamentales

Des spécificités à chaque publication (objets taggés et =g0= pour A&A, les données à mettre en =e= dans l'ApJS,...)

MISSION DE BASE

Attacher les objets aux références de la littérature scientifique

Créer les références bibliographiques le cas échéant

Dispatcher les références aux autres équipes (Dictionnaire, VizieR, Cosim) et aux astronomes pour expertise scientifique et mise à jour des données fondamentales

Des spécificités à chaque publication (objets taggés et =g0= pour A&A, …)

En raison de notre place dans la chaîne documentaire, nous sommes amenés à constater et signaler des erreurs/problèmes, dans Simbad, dans la mise à jour, quand on les remarque mais n'oubliez pas :

18 articles par jour

La notice bibliographique « BIBCODE »

DJIN, mais pas seulement

*** Récupérée de l'Editeur (A&A, ApJ, AJ, MNRAS, PASP,…)**

*** Créée via DJIN1**

*** Créée manuellement (PASJ, Atel,…)**
Programme pour le faire de manière automatique en cours

TRAITER UN ARTICLE
Sans DJIN

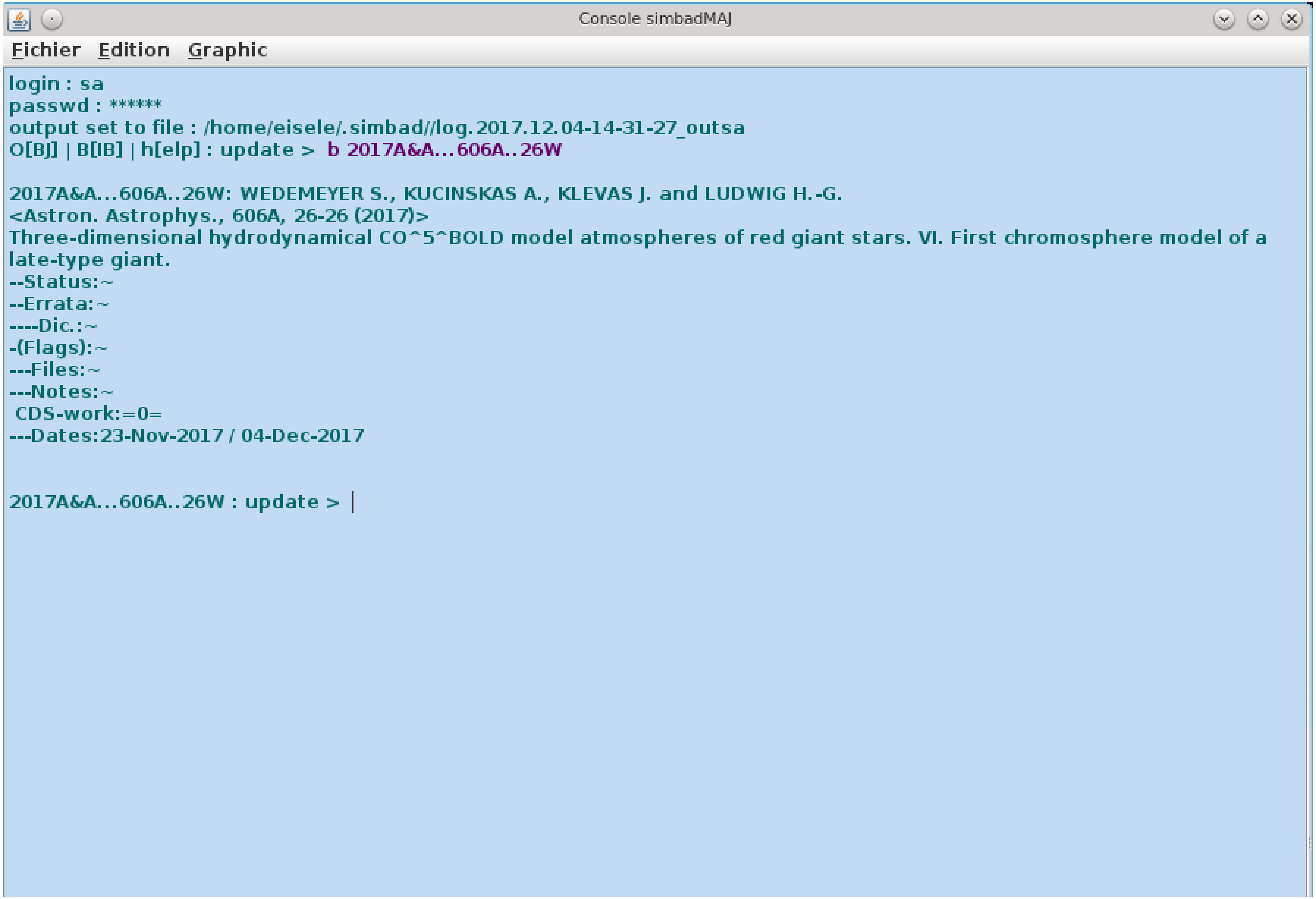

TRAITER UN ARTICLE
Sans DJIN

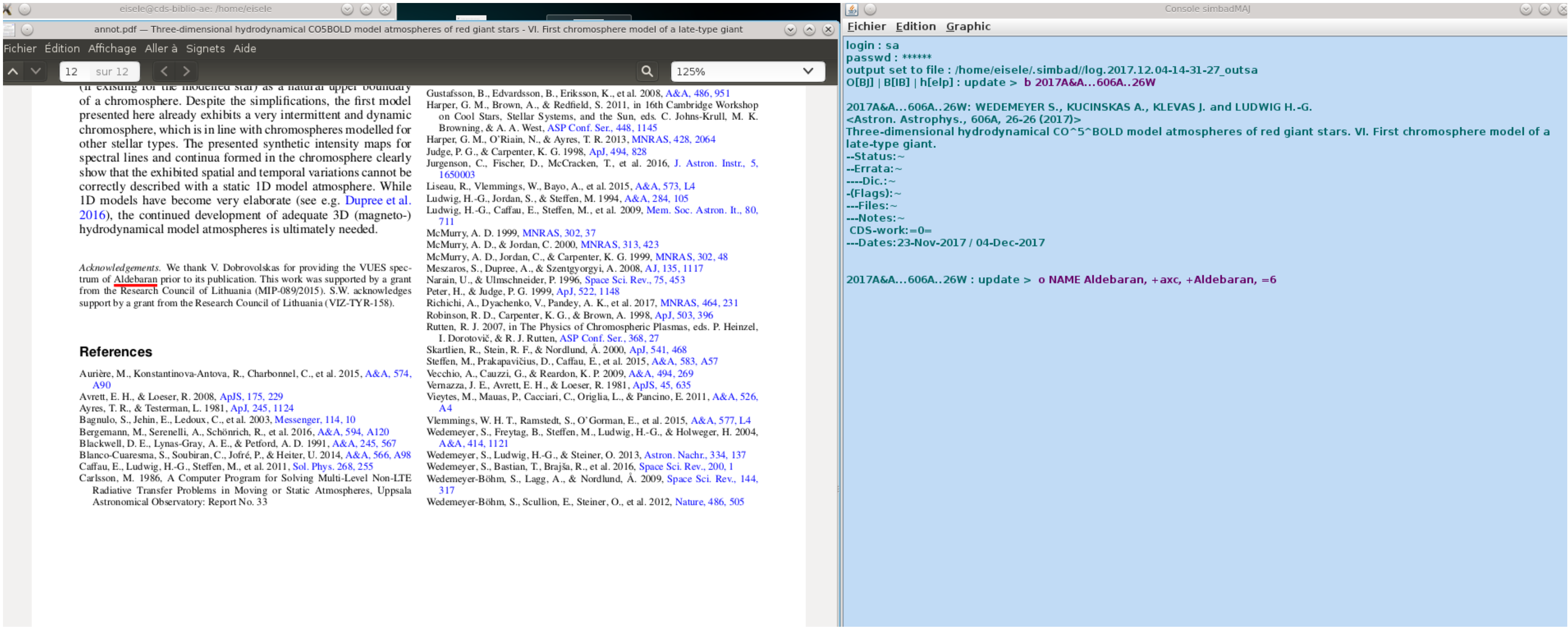

TRAITER UN ARTICLE
Sans DJIN

Console simbadMAJ

Fichier Edition Graphic

```
login : sa
passwd : ******
output set to file : /home/eisele/.simbad//log.2017.12.04-14-31-27_outsa
O[BJ] | B[IB] | h[elp] : update >  b 2017A&A...606A..26W

2017A&A...606A..26W: WEDEMEYER S., KUCINSKAS A., KLEVAS J. and LUDWIG H.-G.
<Astron. Astrophys., 606A, 26-26 (2017)>
Three-dimensional hydrodynamical CO^5^BOLD model atmospheres of red giant stars. VI. First chromosphere model of a
late-type giant.
--Status:~
--Errata:~
----Dic.:~
-(Flags):~
---Files:~
---Notes:~
 CDS-work:=0=
---Dates:23-Nov-2017 / 04-Dec-2017


2017A&A...606A..26W : update >  o NAME Aldebaran, +axc, +Aldebaran, =6
```

Console simbadMAJ

Fichier Edition Graphic

```
login : sa
passwd : ******
output set to file : /home/eisele/.simbad//log.2017.12.04-14-34-40_outsa
O[BJ] | B[IB] | h[elp] : update >  b 2017A&A...606A..26W

2017A&A...606A..26W: WEDEMEYER S., KUCINSKAS A., KLEVAS J. and LUDWIG H.-G.
<Astron. Astrophys., 606A, 26-26 (2017)>
Three-dimensional hydrodynamical CO^5^BOLD model atmospheres of red giant stars. VI. First chromosphere model of a
late-type giant.
--Status:~
--Errata:~
----Dic.:~
-(Flags):~
---Files:~
---Notes:~
 CDS-work:=0=
---Dates:23-Nov-2017 / 04-Dec-2017


2017A&A...606A..26W : update >  o NAME Aldebaran, +axc, +Aldebaran, =6
Ajout du lien :NAME Aldebaran / 2017A&A...606A..26W
=================================
* alf Tau (cl)
============= Type: LP?  Long Period Variable candidate
Coord ICRS(2000): 04 35 55.23907+16 30 33.4885 (Opt ) [7.38 5.70 90] A 2007A&A...474..653V
Coord ICRS(1950): 04 35 55.01847+16 30 42.9355 (Opt ) [7.38 5.70 90] A 2007A&A...474..653V
Coord FK5(2000): 04 35 55.239+16 30 33.49 (Opt ) [7.38 5.70 90] A 2007A&A...474..653V
Coord FK5(1950): 04 33 02.909+16 24 37.57 (Opt ) [7.38 5.70 90] A 2007A&A...474..653V
 gal= 180.9719-20.2483
 sgal= 338.1258-42.9367
 ecl= 069.0901174-05.4709055 [A] 2007A&A...474..653V
Coord FK4(1950): 04 33 02.89+16 24 37.6 (Opt ) [7.38 5.70 90] A 2007A&A...474..653V
=======================================
 mb, mv = 2.40 0.86   ---  morph. type = ~ ~ ~ / spectral K5+III B 1989ApJS...71..245K
=======================================
 dim =     ~     ~    ~ (I)
=======================================
 rv = v   54.26    A [+-0.03] 2005A&A...430..165F
Do you want to see more ? n

NAME Aldebaran : update >  v

2017A&A...606A..26W : update OBJ >
```

TRAITER UN ARTICLE
Avec DJIN

1) Ouvrir avec DJIN

2)Eliminer le bruit

3)Lecture de l'article en diagonale

4)Identification des objets restants

5)Verify

6)Simulation

7)Exécution

Ouvrir avec DJIN

TRAITER UN ARTICLE

1) Ouvrir avec DJIN

2) Eliminer le bruit

3)Lecture de l'article en diagonale

4)Identification des objets restants

5)Verify

6)Simulation

7)Exécution

Éliminer le bruit

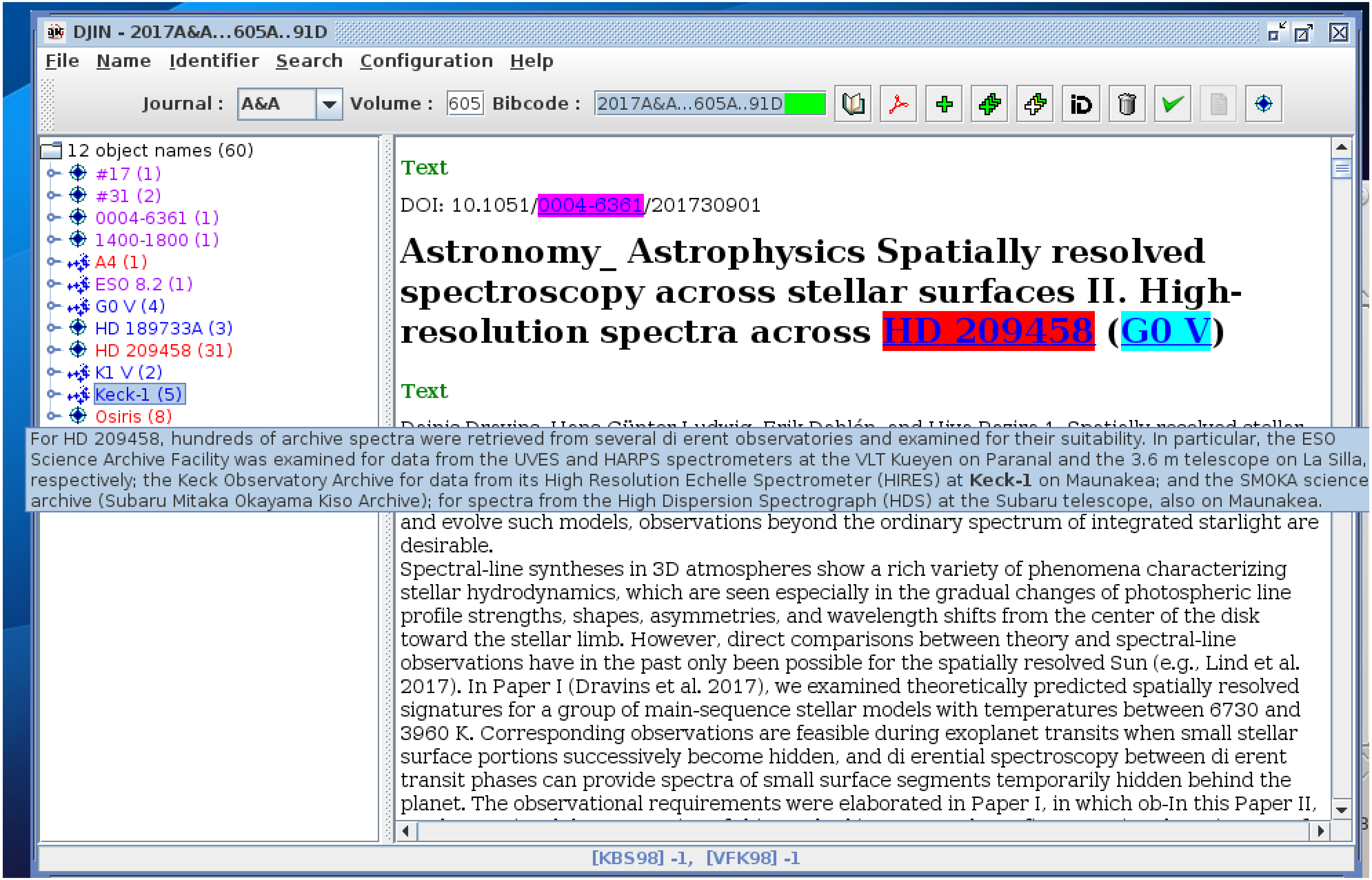

Éliminer le bruit

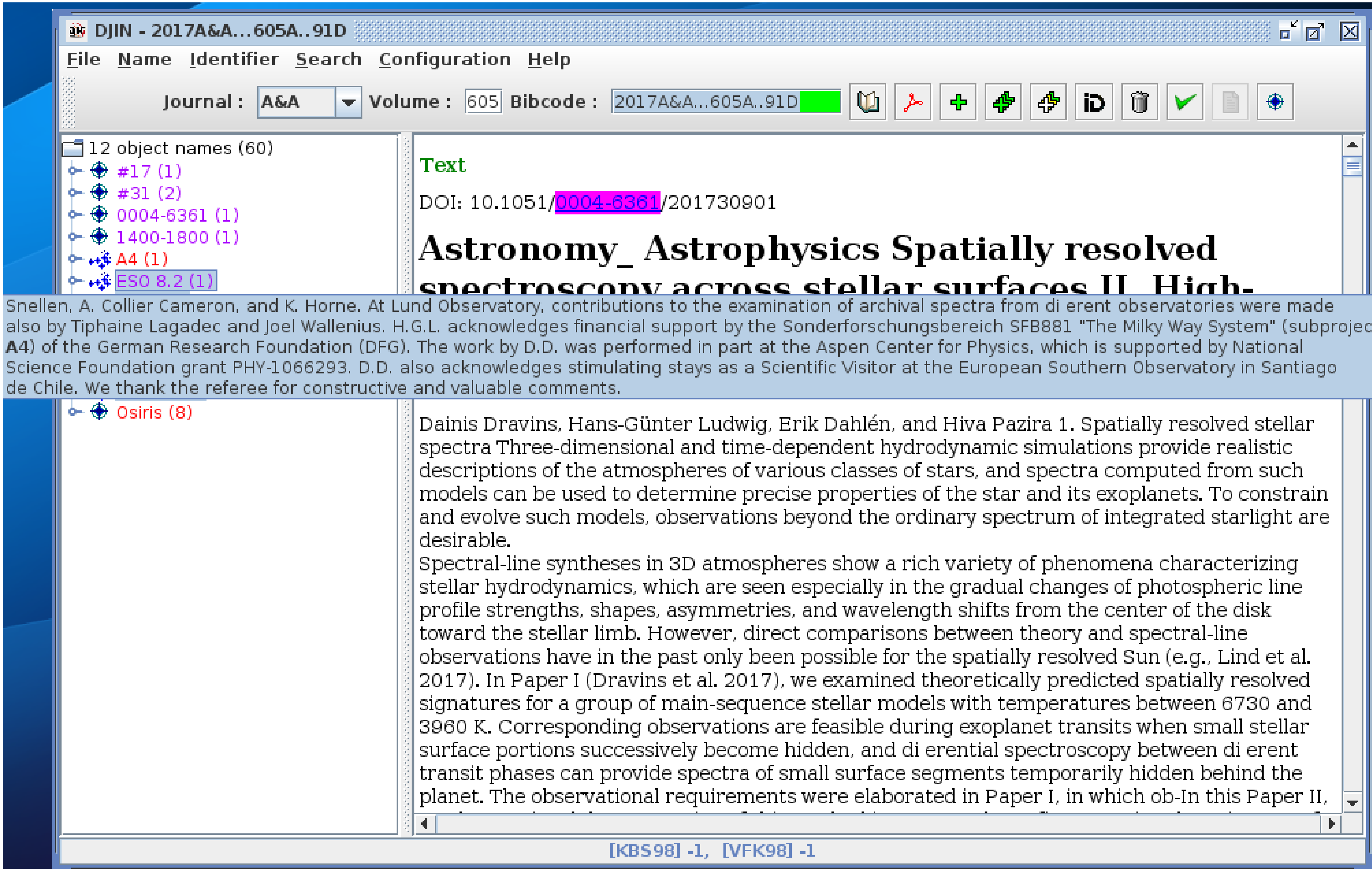

Éliminer le bruit

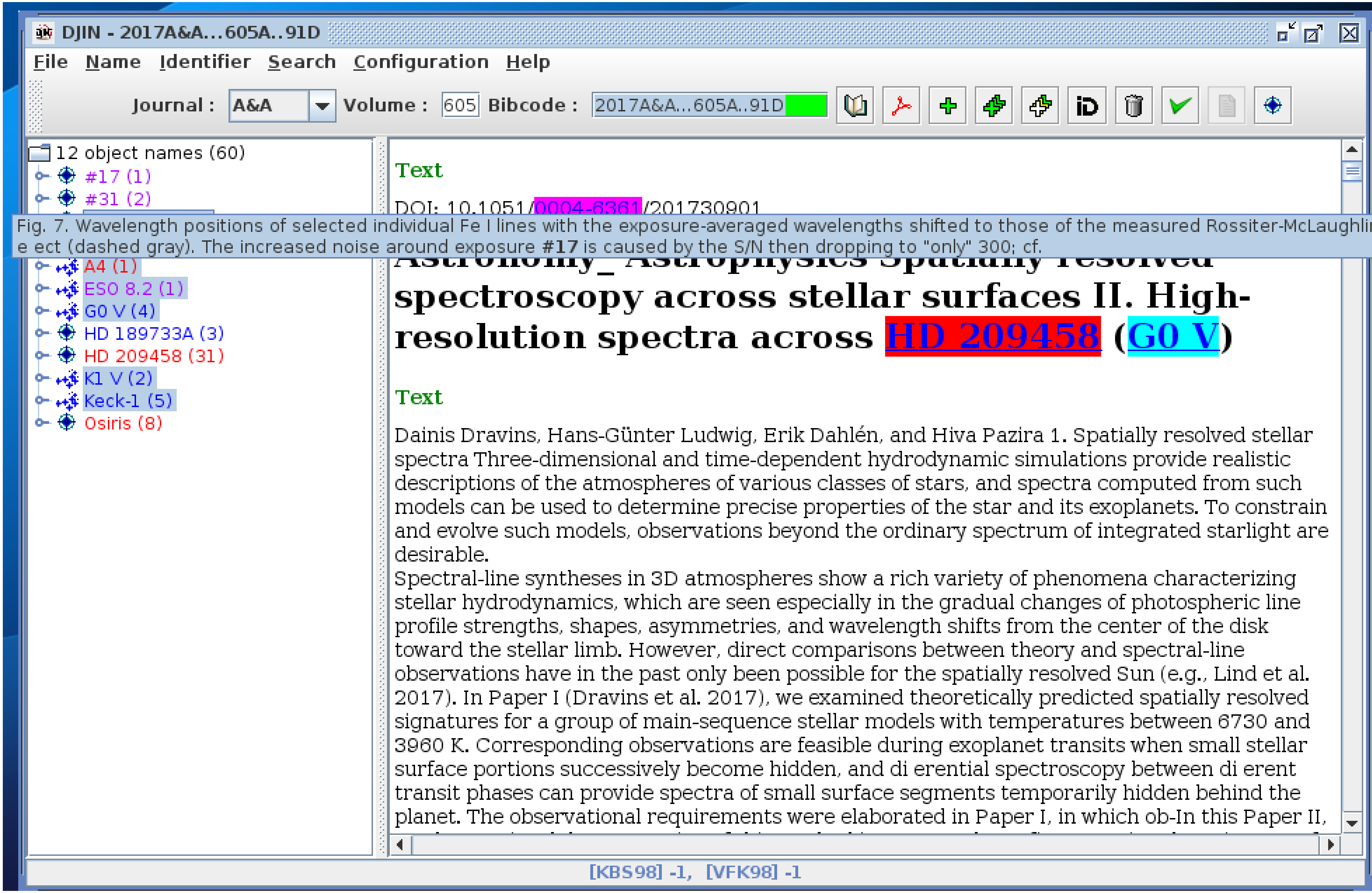

Éliminer le bruit : résultat

TRAITER UN ARTICLE

1) Ouvrir avec DJIN

2)Eliminer le bruit

3)Lecture de l’article en diagonale

4)Identification des objets restants

5)Verify

6)Simulation

7)Exécution

TRAITER UN ARTICLE

1) Ouvrir avec DJIN

2)Eliminer le bruit

3)Lecture de l'article en diagonale

Repérage des -oublis/mauvaises détections de DJIN
-tables
-données disponibles en ligne
-données à ajouter aux objets

4)Identification des objets restants

5)Verify

6)Simulation

7)Exécution

Lecture de l'article en diagonal

annot.pdf — Spatially resolved spectroscopy across stellar surfaces - II. High-resolution spectra across HD 209458 (G0 V)

Fichier Édition Affichage Aller à Signets Aide

7 sur 12 125%

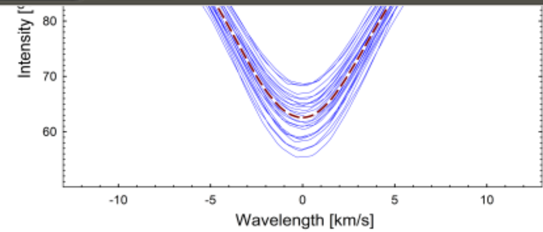

Fig. 8. Averaging 26 "similar" photospheric Fe I lines in HD 209458, selected to be largely unblended and of closely similar strengths (Fig. 5). Their average (dashed) "synthesizes" a representative profile of such a strength in that particular wavelength region. For this reference profile averaged over several exposures outside transit, the photometric signal-to-noise ratio approaches ~7000.

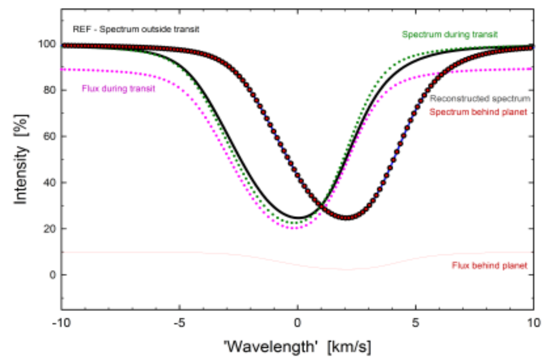

Fig. 9. Different spectral-line components treated in the reconstruction of spatially resolved spectra. The spectrum behind the planet is obtained as that line profile (weighted with the amount of flux temporarily obscured by the planet) that – summed with the temporarily observed line profile – produces the stellar reference profile outside of transit. For clarity, the planetary signal here is greatly exaggerated.

HD 209458 by Hayek et al. (2012) from 3D stellar model atmospheres in passbands including the red SDSS r', whose effective wavelength of 620.4 nm (Fukugita et al. 1996) closely coincides with the average for our spectral-line selections. However, we stress that our method of spatially resolved line reconstruction does not depend on any theoretical predictions of limb darkening; only the product of planetary area and stellar local brightness is required and such data could be taken directly from observed transit photometry. Separating the values for the planet area and limb darkening makes it easier to discuss error budgets, and a limb-darkening model enables us to extrapolate continuum intensities to the stellar disk center that is not sampled during the exoplanet transit.

6.2. Reconstructing spatially resolved profiles

The principle for profile reconstruction is shown in Fig. 9. The spectroscopically observed profiles are different from each

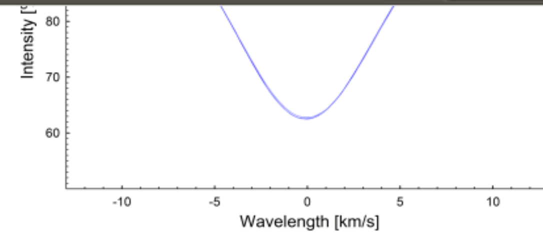

Fig. 10. Representative profiles of the weaker Fe I line and its gradual changes. Each profile, which is the average of 26 Fe I lines, is plotted for 14 successive exposures during the exoplanet transit, showing the degree of uniformity reached. To appreciate the slight changes during the transit, this plot should be viewed highly magnified; corresponding line ratios are in Fig. 11. The photometric signal-to-noise ratio here is ~2500.

transit phase and from the reference profile from outside transit. The diminution of the flux at each transit phase is taken from limb-darkening functions and planet-size determinations fitted to independent photometric observations. The spectrum behind the planet is obtained as that line profile, weighted with the appropriate fractional flux, that, together with the then observed line profile, produces the profile without a planet outside transit. The resulting spectral continuum level can be expressed relative to the intensity at stellar disk center or to the full-disk average (thus showing effects of limb darkening) or it can be normalized to a local intensity of 100% in the more common spectral format. In this illustration, the impact of the planet is exaggerated by an order of magnitude: even large planets do not cover much more than 1% of the surface of solar-type stars.

6.3. Transit sequence of averaged Fe I profiles

Figure 10 shows an overplot of the averaged weaker Fe I line for 14 successive exposures during the Osiris transit. Compared to the schematics of Fig. 9, the spectral-line variations in the actual data are tiny. Here, the averaging over 26 different lines produces a photometric $S/N \sim 2500$ that begins to be useful when combined with the still lower noise reference profile from outside transit. While this plot shows the degree of uniformity reached, the differences between successive exposures are too subtle to be easily appreciated. These are better seen in Fig. 11, which shows the successive ratios of each line profile to the reference profile, in the same format at the theoretical curves in Figs. 9 and 10 of Paper I.

6.4. Reconstructed line profiles

To compute the flux temporarily hidden during transit, the projected planet area was taken as 1.5% of the stellar disk, with limb darkening from Hayek et al. (2012) for the passband SDSS r'; these values are deduced from photometry. The center-to-limb position of the planet from the transit trajectory was computed from the impact parameter =0.51, as deduced by various authors from the measured Rossiter-McLaughlin effect.

TRAITER UN ARTICLE

1) Ouvrir avec DJIN

2)Eliminer le bruit

3)Lecture de l'article en diagonale

4) Identification des objets restants

5)Verify

6)Simulation

7)Exécution

TRAITER UN ARTICLE

1) Ouvrir avec DJIN

2)Eliminer le bruit

3)Lecture de l'article en diagonale

4) Identification des objets restants

Différents outils -références citées dans l'article
-Coordonnées
-Dictionnaire
-NED
-gsc4sim
-Google
-...

5)Verify

6)Simulation

7)Exécution

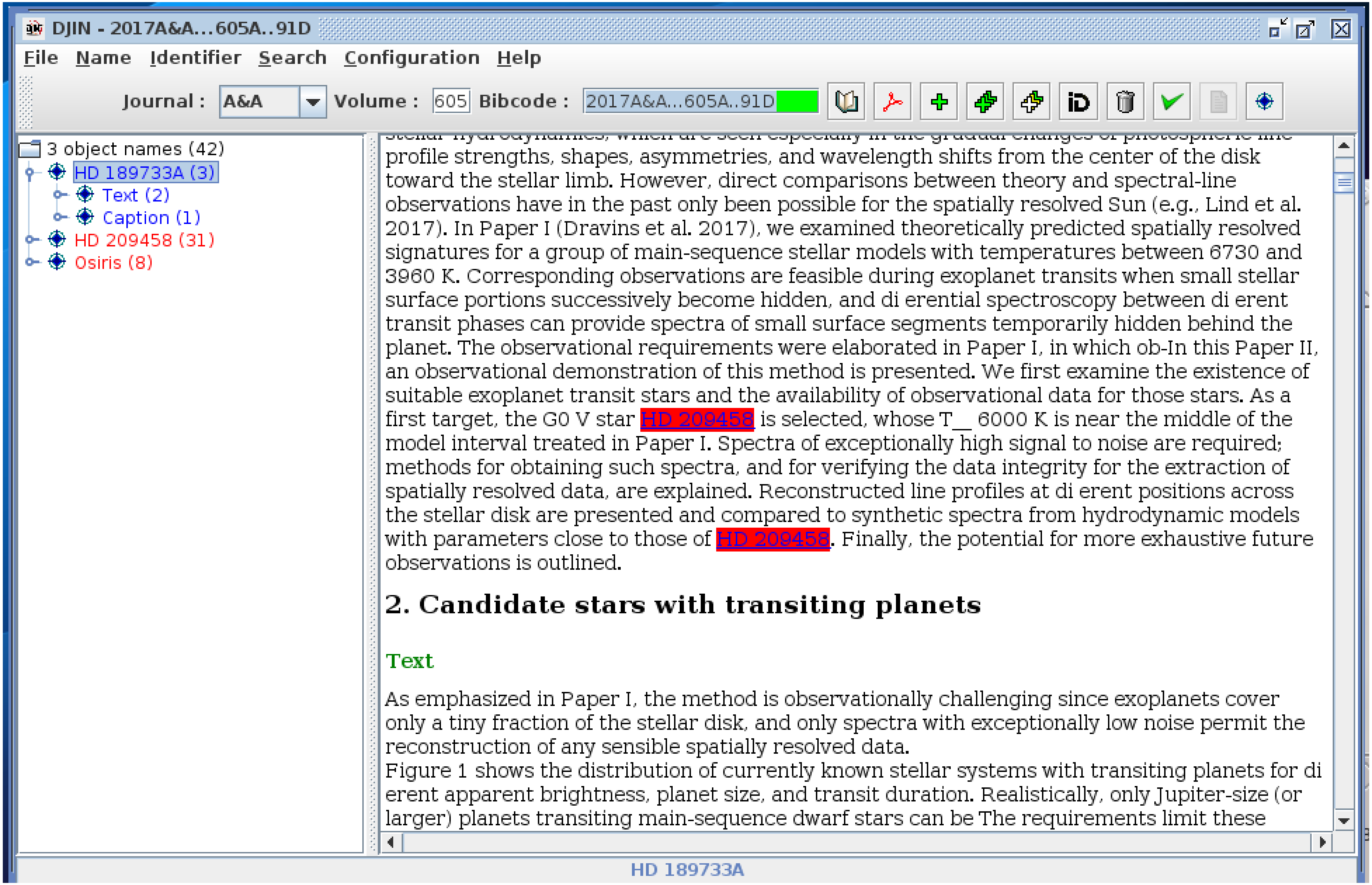
DJIN - 2017A&A...605A..91D
File Name Identifier Search Configuration Help
Journal : A&A Volume : 605 Bibcode : 2017A&A...605A..91D
3 object names (42)
HD 189733A (3)
Text (2)
Caption (1)
HD 209458 (31)
Osiris (8)
profile strengths, shapes, asymmetries, and wavelength shifts from the center of the disk toward the stellar limb. However, direct comparisons between theory and spectral-line observations have in the past only been possible for the spatially resolved Sun (e.g., Lind et al. 2017). In Paper I (Dravins et al. 2017), we examined theoretically predicted spatially resolved signatures for a group of main-sequence stellar models with temperatures between 6730 and 3960 K. Corresponding observations are feasible during exoplanet transits when small stellar surface portions successively become hidden, and di erential spectroscopy between di erent transit phases can provide spectra of small surface segments temporarily hidden behind the planet. The observational requirements were elaborated in Paper I, in which ob-In this Paper II, an observational demonstration of this method is presented. We first examine the existence of suitable exoplanet transit stars and the availability of observational data for those stars. As a first target, the G0 V star HD 209458 is selected, whose T__ 6000 K is near the middle of the model interval treated in Paper I. Spectra of exceptionally high signal to noise are required; methods for obtaining such spectra, and for verifying the data integrity for the extraction of spatially resolved data, are explained. Reconstructed line profiles at di erent positions across the stellar disk are presented and compared to synthetic spectra from hydrodynamic models with parameters close to those of HD 209458. Finally, the potential for more exhaustive future observations is outlined.
2. Candidate stars with transiting planets
Text
As emphasized in Paper I, the method is observationally challenging since exoplanets cover only a tiny fraction of the stellar disk, and only spectra with exceptionally low noise permit the reconstruction of any sensible spatially resolved data.
Figure 1 shows the distribution of currently known stellar systems with transiting planets for di erent apparent brightness, planet size, and transit duration. Realistically, only Jupiter-size (or larger) planets transiting main-sequence dwarf stars can be The requirements limit these
HD 189733A

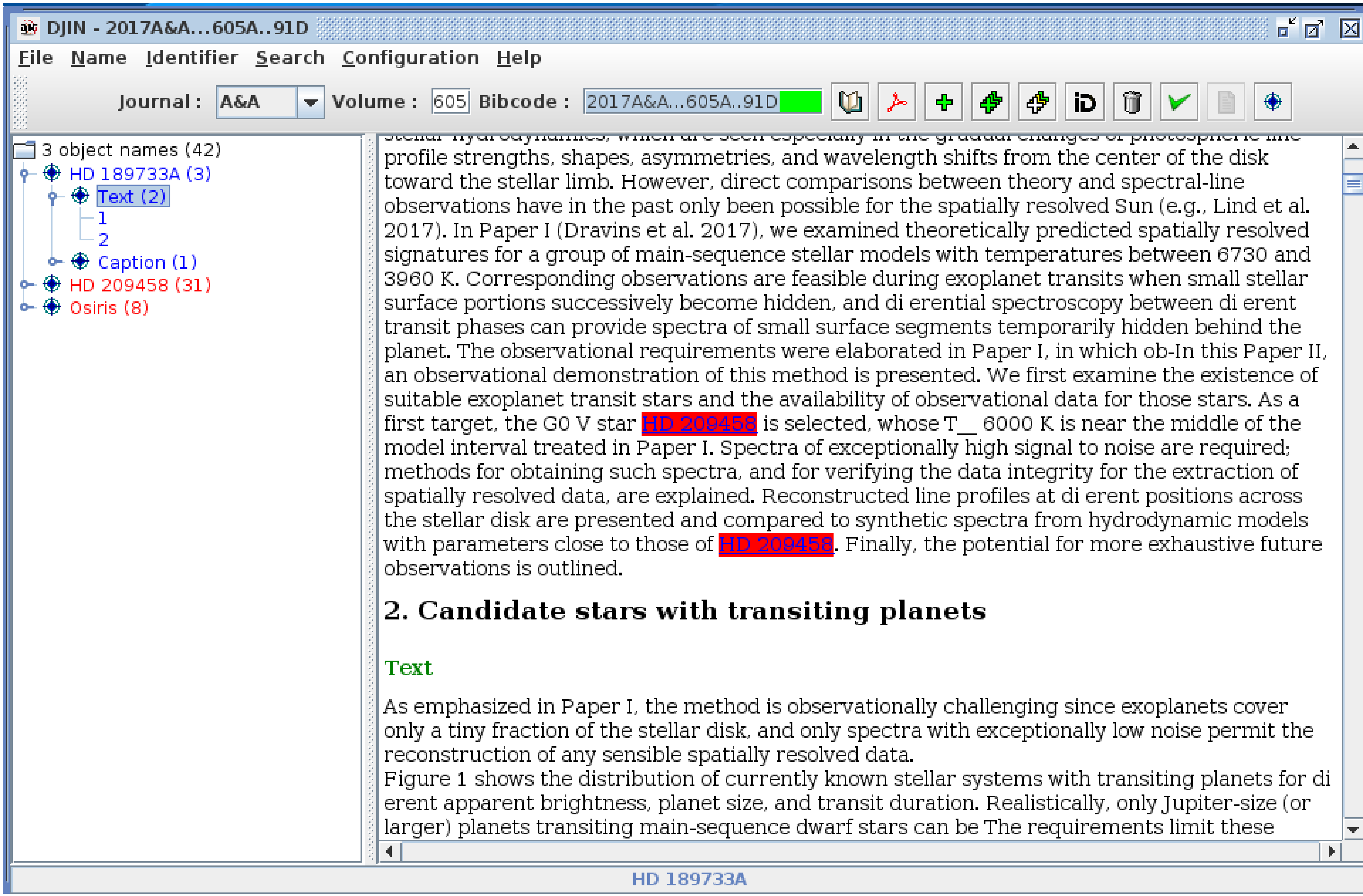
DJIN - 2017A&A...605A..91D
File Name Identifier Search Configuration Help
Journal : A&A Volume : 605 Bibcode : 2017A&A...605A..91D
3 object names (42)
HD 189733A (3)
Text (2)
1
2
Caption (1)
HD 209458 (31)
Osiris (8)
profile strengths, shapes, asymmetries, and wavelength shifts from the center of the disk toward the stellar limb. However, direct comparisons between theory and spectral-line observations have in the past only been possible for the spatially resolved Sun (e.g., Lind et al. 2017). In Paper I (Dravins et al. 2017), we examined theoretically predicted spatially resolved signatures for a group of main-sequence stellar models with temperatures between 6730 and 3960 K. Corresponding observations are feasible during exoplanet transits when small stellar surface portions successively become hidden, and di erential spectroscopy between di erent transit phases can provide spectra of small surface segments temporarily hidden behind the planet. The observational requirements were elaborated in Paper I, in which ob-In this Paper II, an observational demonstration of this method is presented. We first examine the existence of suitable exoplanet transit stars and the availability of observational data for those stars. As a first target, the G0 V star HD 209458 is selected, whose T__ 6000 K is near the middle of the model interval treated in Paper I. Spectra of exceptionally high signal to noise are required; methods for obtaining such spectra, and for verifying the data integrity for the extraction of spatially resolved data, are explained. Reconstructed line profiles at di erent positions across the stellar disk are presented and compared to synthetic spectra from hydrodynamic models with parameters close to those of HD 209458. Finally, the potential for more exhaustive future observations is outlined.
2. Candidate stars with transiting planets
Text
As emphasized in Paper I, the method is observationally challenging since exoplanets cover only a tiny fraction of the stellar disk, and only spectra with exceptionally low noise permit the reconstruction of any sensible spatially resolved data.
Figure 1 shows the distribution of currently known stellar systems with transiting planets for di erent apparent brightness, planet size, and transit duration. Realistically, only Jupiter-size (or larger) planets transiting main-sequence dwarf stars can be The requirements limit these
HD 189733A

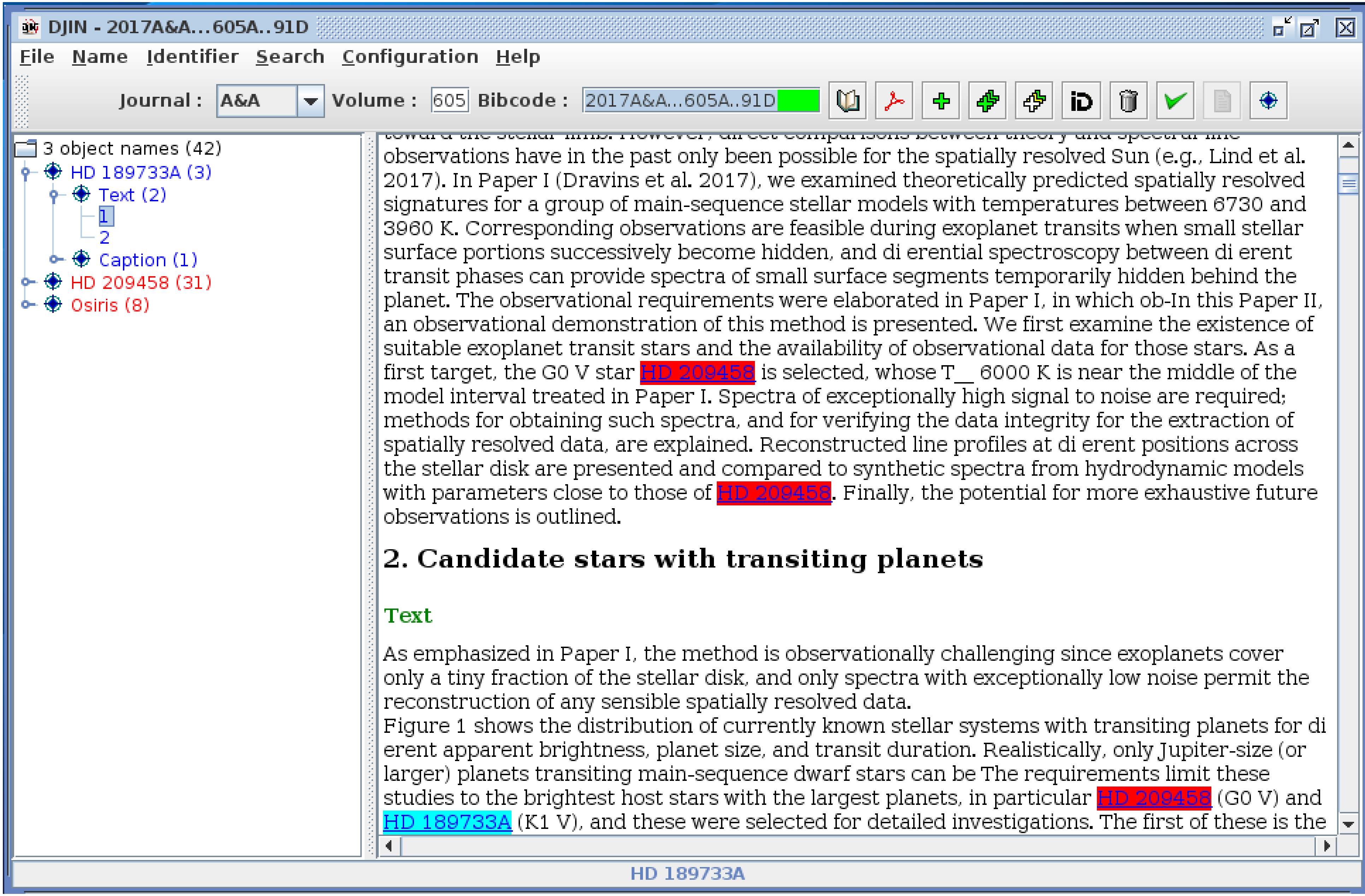
DJIN - 2017A&A...605A..91D
File Name Identifier Search Configuration Help
Journal : A&A Volume : 605 Bibcode : 2017A&A...605A..91D
3 object names (42)
HD 189733A (3)
Text (2)
1
2
Caption (1)
HD 209458 (31)
Osiris (8)
observations have in the past only been possible for the spatially resolved Sun (e.g., Lind et al. 2017). In Paper I (Dravins et al. 2017), we examined theoretically predicted spatially resolved signatures for a group of main-sequence stellar models with temperatures between 6730 and 3960 K. Corresponding observations are feasible during exoplanet transits when small stellar surface portions successively become hidden, and di erential spectroscopy between di erent transit phases can provide spectra of small surface segments temporarily hidden behind the planet. The observational requirements were elaborated in Paper I, in which ob-In this Paper II, an observational demonstration of this method is presented. We first examine the existence of suitable exoplanet transit stars and the availability of observational data for those stars. As a first target, the G0 V star HD 209458 is selected, whose T__ 6000 K is near the middle of the model interval treated in Paper I. Spectra of exceptionally high signal to noise are required; methods for obtaining such spectra, and for verifying the data integrity for the extraction of spatially resolved data, are explained. Reconstructed line profiles at di erent positions across the stellar disk are presented and compared to synthetic spectra from hydrodynamic models with parameters close to those of HD 209458. Finally, the potential for more exhaustive future observations is outlined.
2. Candidate stars with transiting planets
Text
As emphasized in Paper I, the method is observationally challenging since exoplanets cover only a tiny fraction of the stellar disk, and only spectra with exceptionally low noise permit the reconstruction of any sensible spatially resolved data.
Figure 1 shows the distribution of currently known stellar systems with transiting planets for di erent apparent brightness, planet size, and transit duration. Realistically, only Jupiter-size (or larger) planets transiting main-sequence dwarf stars can be The requirements limit these studies to the brightest host stars with the largest planets, in particular HD 209458 (G0 V) and HD 189733A (K1 V), and these were selected for detailed investigations. The first of these is the
HD 189733A

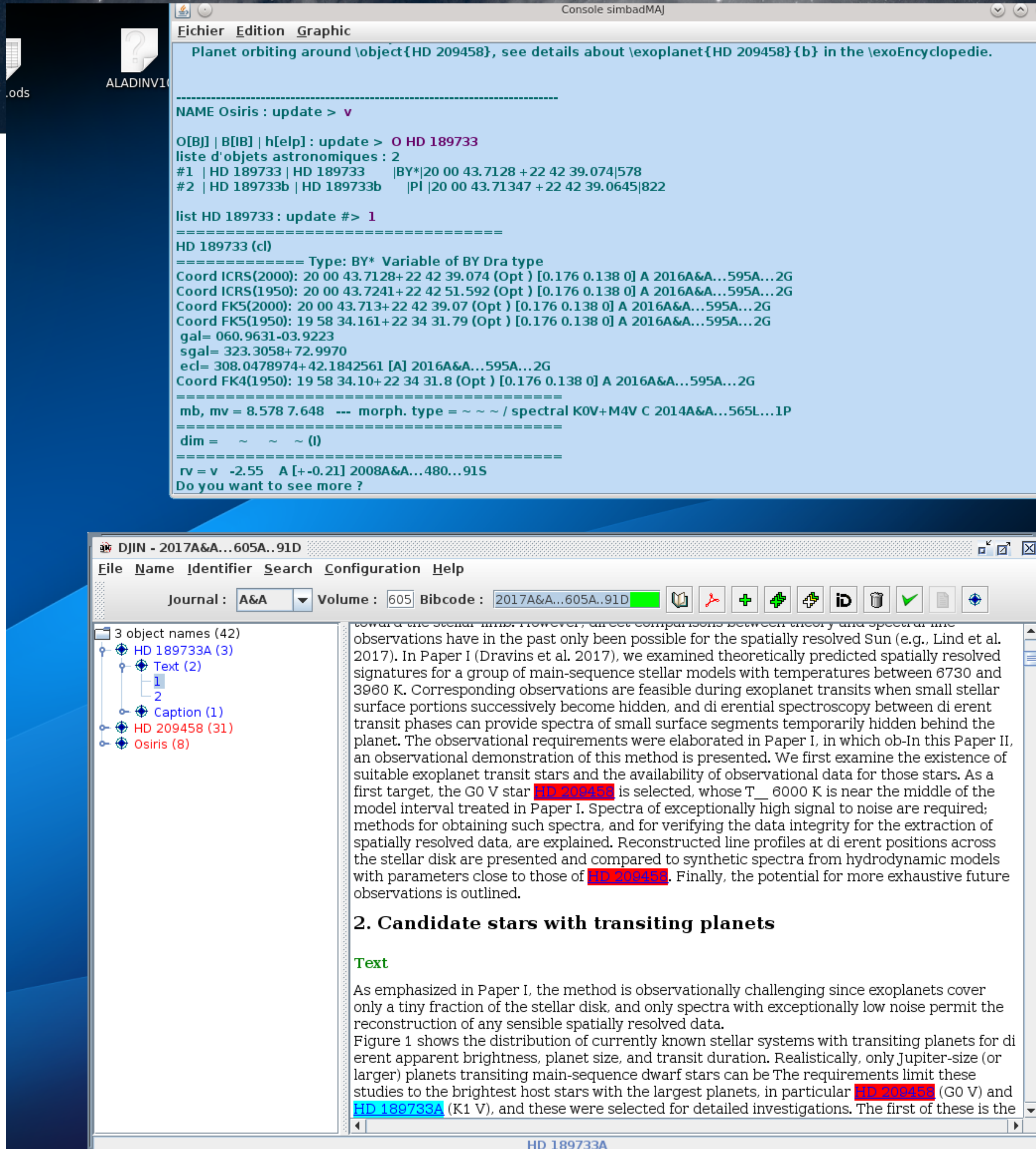
Console simbadMAJ
Fichier Edition Graphic
Planet orbiting around \object{HD 209458}, see details about \exoplanet{HD 209458}{b} in the \exoEncyclopedie.
NAME Osiris : update > v
O[BJ] | B[IB] | h[elp] : update > O HD 189733
liste d'objets astronomiques : 2
#1 | HD 189733 | HD 189733 |BY*|20 00 43.7128 +22 42 39.074|578
#2 | HD 189733b | HD 189733b |Pl |20 00 43.71347 +22 42 39.0645|822
list HD 189733 : update #> 1
HD 189733 (cl)
============= Type: BY* Variable of BY Dra type
Coord ICRS(2000): 20 00 43.7128+22 42 39.074 (Opt) [0.176 0.138 0] A 2016A&A...595A...2G
Coord ICRS(1950): 20 00 43.7241+22 42 51.592 (Opt) [0.176 0.138 0] A 2016A&A...595A...2G
Coord FK5(2000): 20 00 43.713+22 42 39.07 (Opt) [0.176 0.138 0] A 2016A&A...595A...2G
Coord FK5(1950): 19 58 34.161+22 34 31.79 (Opt) [0.176 0.138 0] A 2016A&A...595A...2G
gal= 060.9631-03.9223
sgal= 323.3058+72.9970
ecl= 308.0478974+42.1842561 [A] 2016A&A...595A...2G
Coord FK4(1950): 19 58 34.10+22 34 31.8 (Opt) [0.176 0.138 0] A 2016A&A...595A...2G
mb, mv = 8.578 7.648 --- morph. type = ~ ~ ~ / spectral K0V+M4V C 2014A&A...565L...1P
dim = ~ ~ ~ (I)
rv = v -2.55 A [+-0.21] 2008A&A...480...91S
Do you want to see more ?
DJIN - 2017A&A...605A..91D
File Name Identifier Search Configuration Help
Journal : A&A Volume : 605 Bibcode : 2017A&A...605A..91D
3 object names (42)
HD 189733A (3)
Text (2)
1
2
Caption (1)
HD 209458 (31)
Osiris (8)
observations have in the past only been possible for the spatially resolved Sun (e.g., Lind et al. 2017). In Paper I (Dravins et al. 2017), we examined theoretically predicted spatially resolved signatures for a group of main-sequence stellar models with temperatures between 6730 and 3960 K. Corresponding observations are feasible during exoplanet transits when small stellar surface portions successively become hidden, and di erential spectroscopy between di erent transit phases can provide spectra of small surface segments temporarily hidden behind the planet. The observational requirements were elaborated in Paper I, in which ob-In this Paper II, an observational demonstration of this method is presented. We first examine the existence of suitable exoplanet transit stars and the availability of observational data for those stars. As a first target, the G0 V star HD 209458 is selected, whose T__ 6000 K is near the middle of the model interval treated in Paper I. Spectra of exceptionally high signal to noise are required; methods for obtaining such spectra, and for verifying the data integrity for the extraction of spatially resolved data, are explained. Reconstructed line profiles at di erent positions across the stellar disk are presented and compared to synthetic spectra from hydrodynamic models with parameters close to those of HD 209458. Finally, the potential for more exhaustive future observations is outlined.
2. Candidate stars with transiting planets
Text
As emphasized in Paper I, the method is observationally challenging since exoplanets cover only a tiny fraction of the stellar disk, and only spectra with exceptionally low noise permit the reconstruction of any sensible spatially resolved data.
Figure 1 shows the distribution of currently known stellar systems with transiting planets for di erent apparent brightness, planet size, and transit duration. Realistically, only Jupiter-size (or larger) planets transiting main-sequence dwarf stars can be The requirements limit these studies to the brightest host stars with the largest planets, in particular HD 209458 (G0 V) and HD 189733A (K1 V), and these were selected for detailed investigations. The first of these is the
HD 189733A

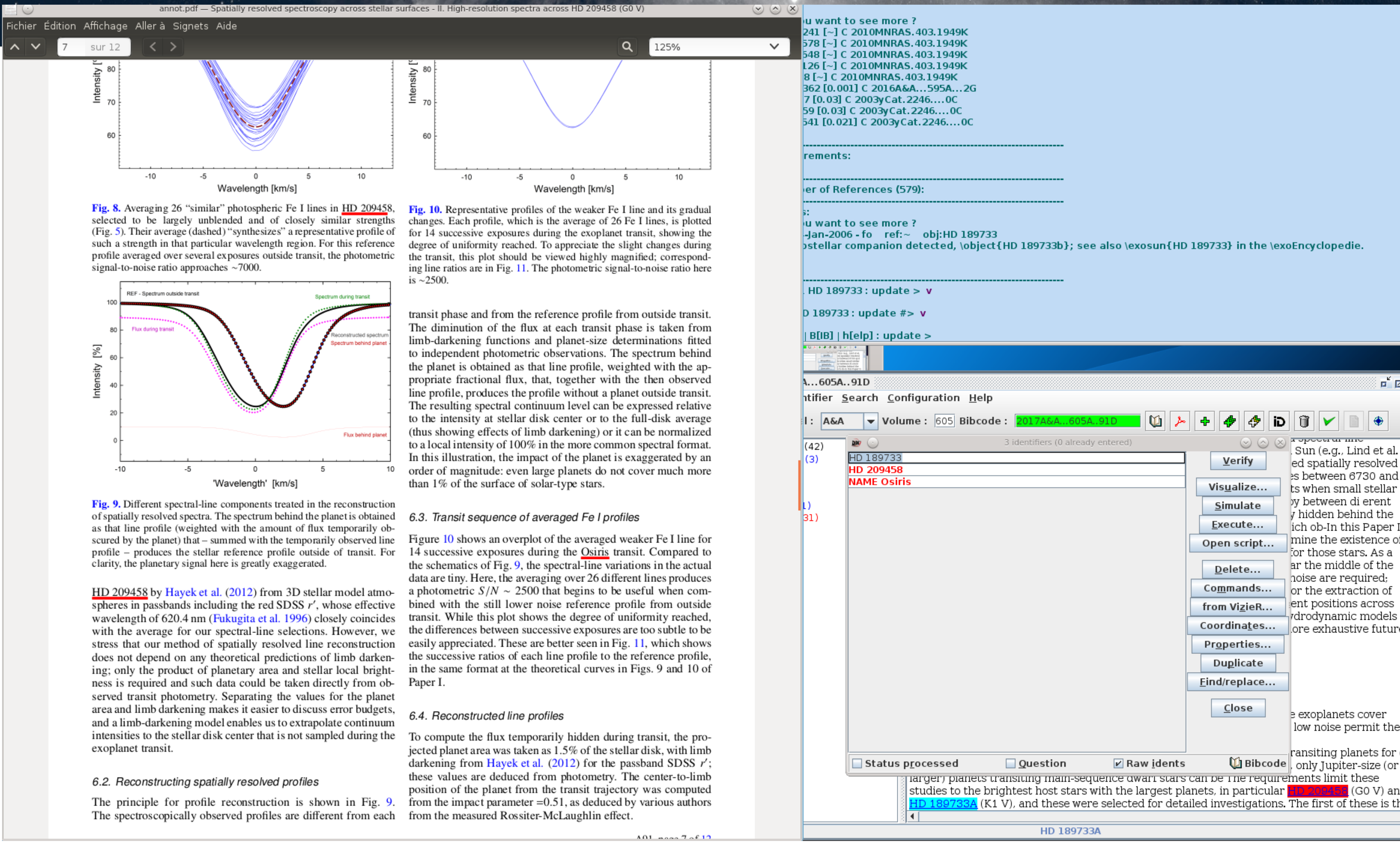

Fig. 8. Averaging 26 "similar" photospheric Fe I lines in HD 209458, selected to be largely unblended and of closely similar strengths (Fig. 5). Their average (dashed) "synthesizes" a representative profile of such a strength in that particular wavelength region. For this reference profile averaged over several exposures outside transit, the photometric signal-to-noise ratio approaches ~7000.

Fig. 9. Different spectral-line components treated in the reconstruction of spatially resolved spectra. The spectrum behind the planet is obtained as that line profile (weighted with the amount of flux temporarily obscured by the planet) that – summed with the temporarily observed line profile – produces the stellar reference profile outside of transit. For clarity, the planetary signal here is greatly exaggerated.

HD 209458 by Hayek et al. (2012) from 3D stellar model atmospheres in passbands including the red SDSS r', whose effective wavelength of 620.4 nm (Fukugita et al. 1996) closely coincides with the average for our spectral-line selections. However, we stress that our method of spatially resolved line reconstruction does not depend on any theoretical predictions of limb darkening; only the product of planetary area and stellar local brightness is required and such data could be taken directly from observed transit photometry. Separating the values for the planet area and limb darkening makes it easier to discuss error budgets, and a limb-darkening model enables us to extrapolate continuum intensities to the stellar disk center that is not sampled during the exoplanet transit.

6.2. Reconstructing spatially resolved profiles

The principle for profile reconstruction is shown in Fig. 9. The spectroscopically observed profiles are different from each

Fig. 10. Representative profiles of the weaker Fe I line and its gradual changes. Each profile, which is the average of 26 Fe I lines, is plotted for 14 successive exposures during the exoplanet transit, showing the degree of uniformity reached. To appreciate the slight changes during the transit, this plot should be viewed highly magnified; corresponding line ratios are in Fig. 11. The photometric signal-to-noise ratio here is ~2500.

transit phase and from the reference profile from outside transit. The diminution of the flux at each transit phase is taken from limb-darkening functions and planet-size determinations fitted to independent photometric observations. The spectrum behind the planet is obtained as that line profile, weighted with the appropriate fractional flux, that, together with the observed line profile, produces the profile without a planet outside transit. The resulting spectral continuum level can be expressed relative to the intensity at stellar disk center or to the full-disk average (thus showing effects of limb darkening) or it can be normalized to a local intensity of 100% in the more common spectral format. In this illustration, the impact of the planet is exaggerated by an order of magnitude: even large planets do not cover much more than 1% of the surface of solar-type stars.

6.3. Transit sequence of averaged Fe I profiles

Figure 10 shows an overplot of the averaged weaker Fe I line for 14 successive exposures during the Osiris transit. Compared to the schematics of Fig. 9, the spectral-line variations in the actual data are tiny. Here, the averaging over 26 different lines produces a photometric $S/N \sim 2500$ that begins to be useful when combined with the still lower noise reference profile from outside transit. While this plot shows the degree of uniformity reached, the differences between successive exposures are too subtle to be easily appreciated. These are better seen in Fig. 11, which shows the successive ratios of each line profile to the reference profile, in the same format at the theoretical curves in Figs. 9 and 10 of Paper I.

6.4. Reconstructed line profiles

To compute the flux temporarily hidden during transit, the projected planet area was taken as 1.5% of the stellar disk, with limb darkening from Hayek et al. (2012) for the passband SDSS r'; these values are deduced from photometry. The center-to-limb position of the planet from the transit trajectory was computed from the impact parameter =0.51, as deduced by various authors from the measured Rossiter-McLaughlin effect.

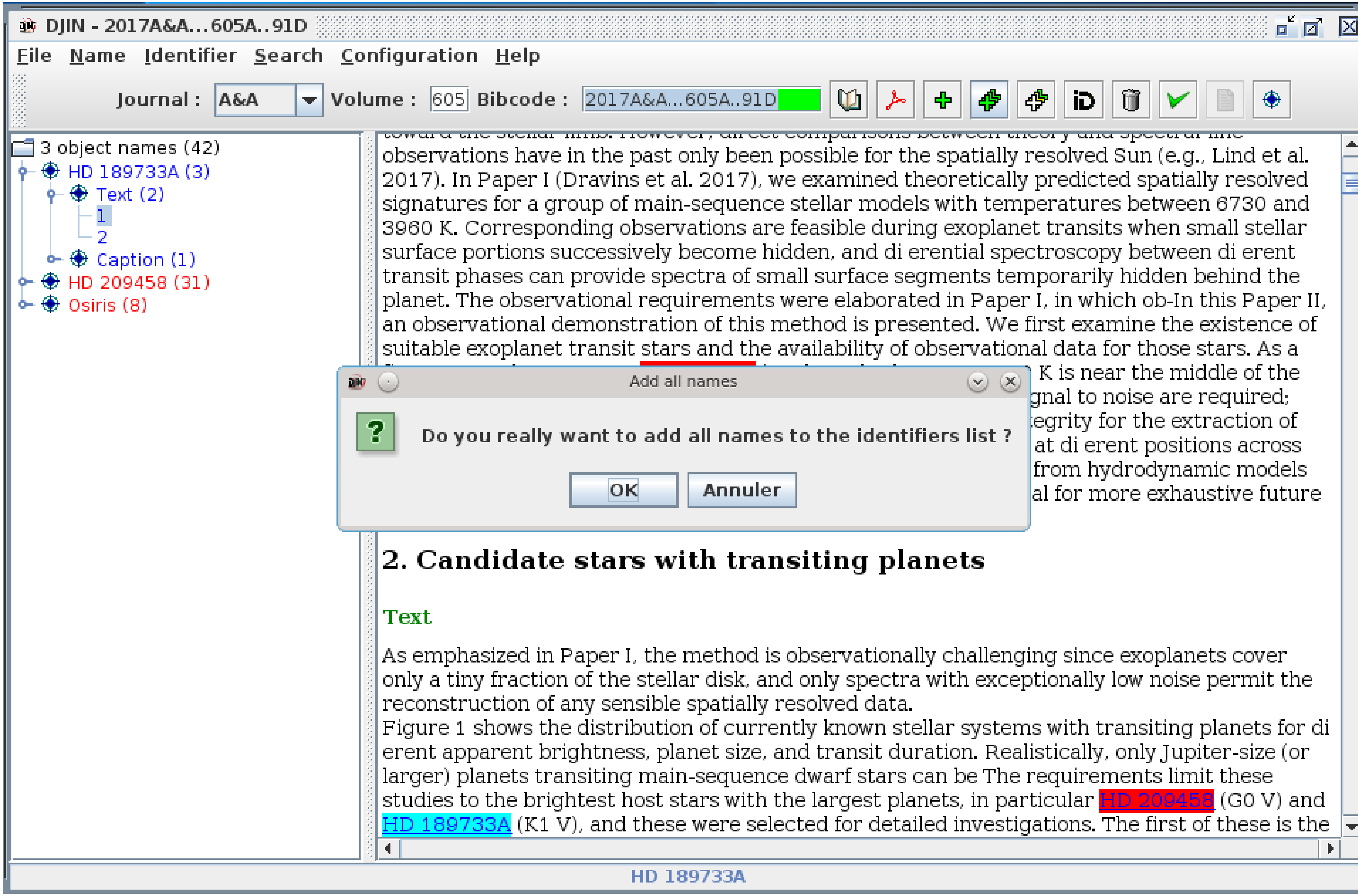
DJIN - 2017A&A...605A..91D
File Name Identifier Search Configuration Help
Journal : A&A Volume : 605 Bibcode : 2017A&A...605A..91D
3 object names (42)
HD 189733A (3)
Text (2)
1
2
Caption (1)
HD 209458 (31)
Osiris (8)
observations have in the past only been possible for the spatially resolved Sun (e.g., Lind et al. 2017). In Paper I (Dravins et al. 2017), we examined theoretically predicted spatially resolved signatures for a group of main-sequence stellar models with temperatures between 6730 and 3960 K. Corresponding observations are feasible during exoplanet transits when small stellar surface portions successively become hidden, and di erential spectroscopy between di erent transit phases can provide spectra of small surface segments temporarily hidden behind the planet. The observational requirements were elaborated in Paper I, in which ob-In this Paper II, an observational demonstration of this method is presented. We first examine the existence of suitable exoplanet transit stars and the availability of observational data for those stars. As a
K is near the middle of the
gnal to noise are required;
egrity for the extraction of
at di erent positions across
from hydrodynamic models
al for more exhaustive future
Add all names
Do you really want to add all names to the identifiers list ?
OK
Annuler
2. Candidate stars with transiting planets
Text
As emphasized in Paper I, the method is observationally challenging since exoplanets cover only a tiny fraction of the stellar disk, and only spectra with exceptionally low noise permit the reconstruction of any sensible spatially resolved data.
Figure 1 shows the distribution of currently known stellar systems with transiting planets for di erent apparent brightness, planet size, and transit duration. Realistically, only Jupiter-size (or larger) planets transiting main-sequence dwarf stars can be The requirements limit these studies to the brightest host stars with the largest planets, in particular HD 209458 (G0 V) and HD 189733A (K1 V), and these were selected for detailed investigations. The first of these is the
HD 189733A

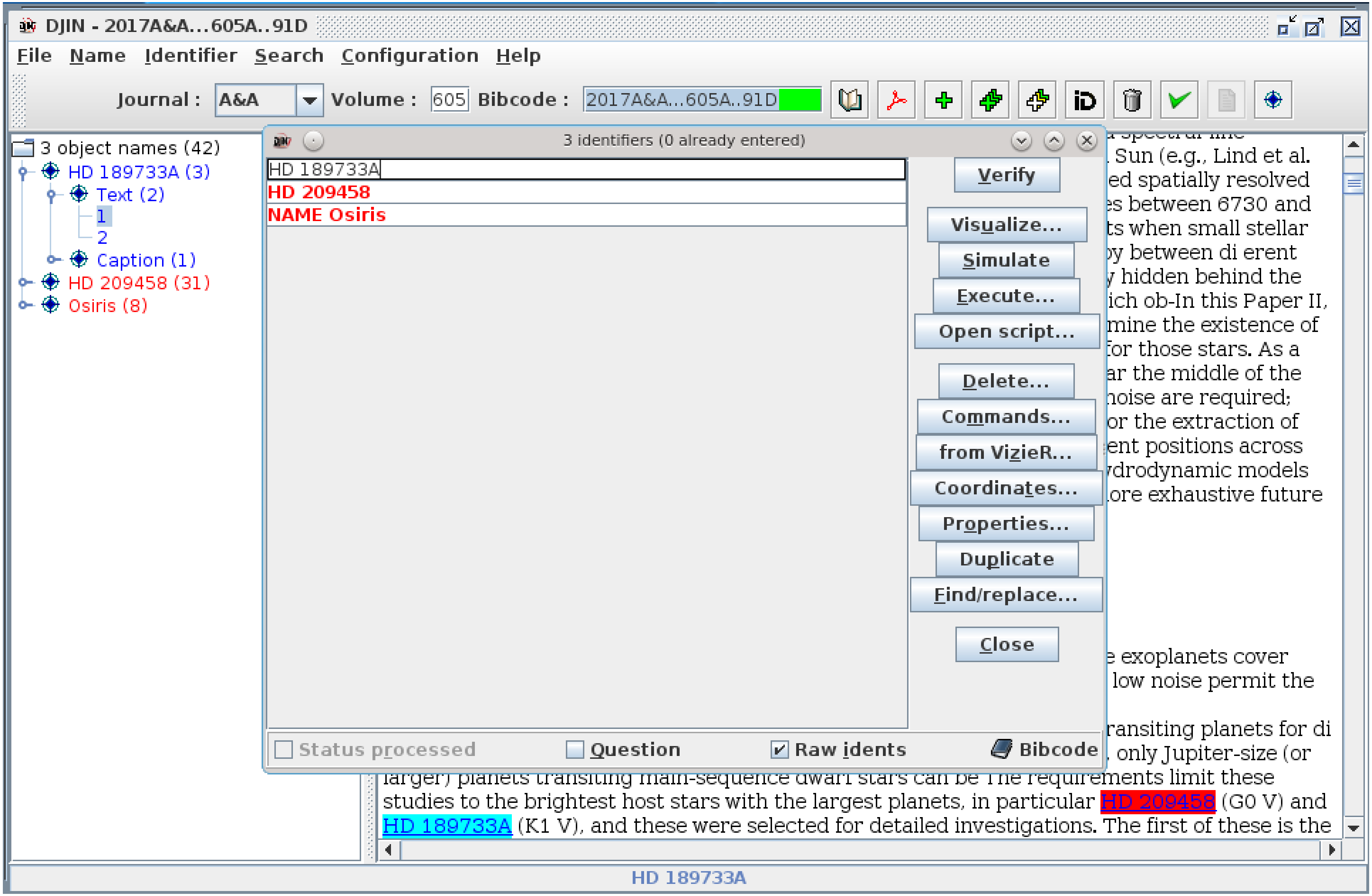
DJIN - 2017A&A...605A..91D
File Name Identifier Search Configuration Help
Journal : A&A Volume : 605 Bibcode : 2017A&A...605A..91D
3 object names (42)
HD 189733A (3)
Text (2)
1
2
Caption (1)
HD 209458 (31)
Osiris (8)
3 identifiers (0 already entered)
HD 189733A
HD 209458
NAME Osiris
Verify
Visualize...
Simulate
Execute...
Open script...
Delete...
Commands...
from VizieR...
Coordinates...
Properties...
Duplicate
Find/replace...
Close
Status processed
Question
Raw idents
Bibcode
studies to the brightest host stars with the largest planets, in particular HD 209458 (G0 V) and
HD 189733A (K1 V), and these were selected for detailed investigations. The first of these is the
HD 189733A

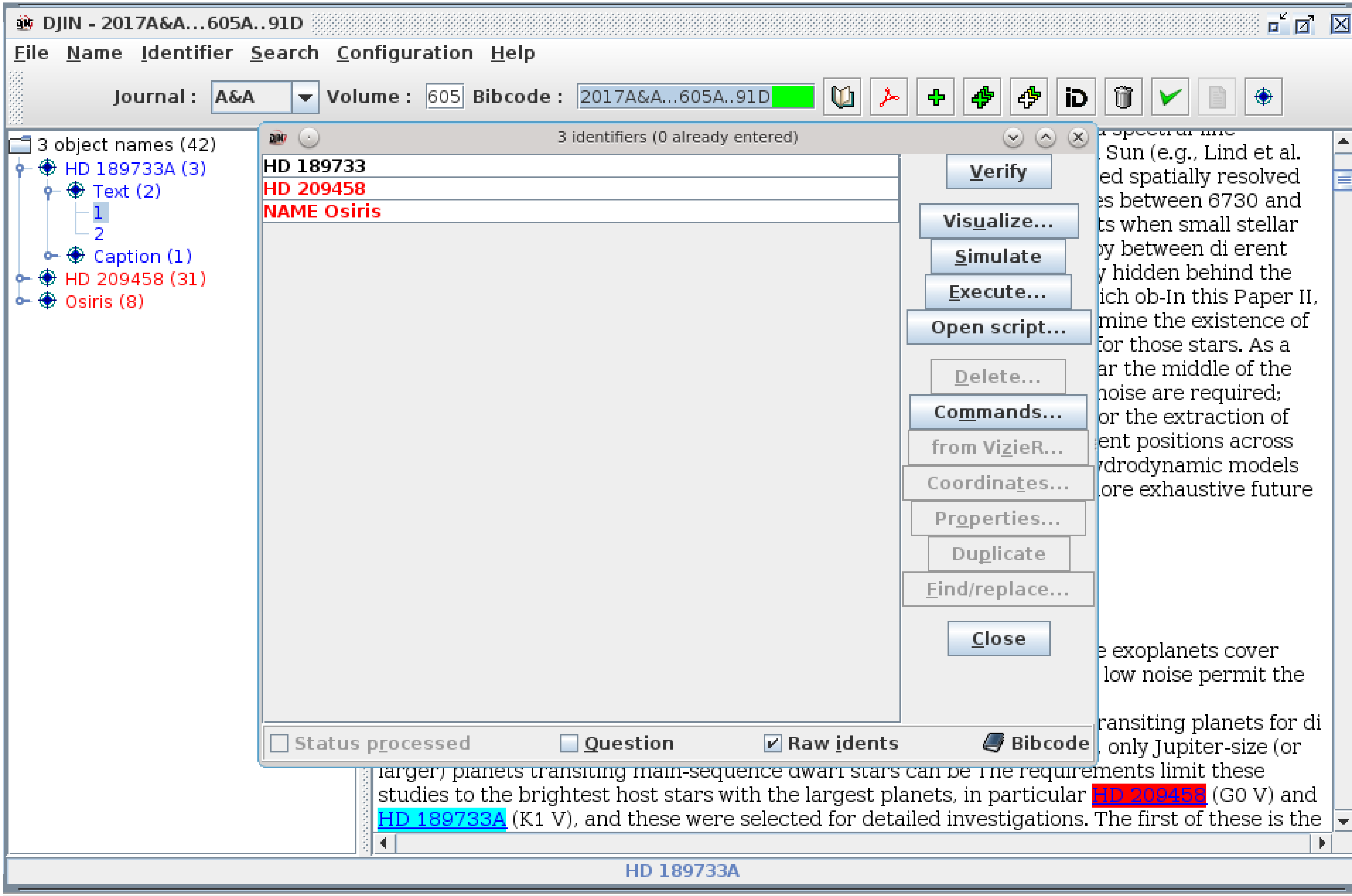
DJIN - 2017A&A...605A..91D
File Name Identifier Search Configuration Help
Journal : A&A Volume : 605 Bibcode : 2017A&A...605A..91D
3 object names (42)
HD 189733A (3)
Text (2)
1
2
Caption (1)
HD 209458 (31)
Osiris (8)
3 identifiers (0 already entered)
HD 189733
HD 209458
NAME Osiris
Verify
Visualize...
Simulate
Execute...
Open script...
Delete...
Commands...
from VizieR...
Coordinates...
Properties...
Duplicate
Find/replace...
Close
Status processed
Question
Raw idents
Bibcode
studies to the brightest host stars with the largest planets, in particular HD 209458 (G0 V) and
HD 189733A (K1 V), and these were selected for detailed investigations. The first of these is the
HD 189733A

TRAITER UN ARTICLE

1) Ouvrir avec DJIN

2)Eliminer le bruit

3)Lecture de l'article en diagonale

4)Identification des objets restants

5)Verify

6)Simulation

7)Exécution

TRAITER UN ARTICLE

1) Ouvrir avec DJIN

2)Eliminer le bruit

3)Lecture de l'article en diagonale

4)Identification des objets restants

5)Verify

Permet de vérifier que les objets existent bien dans SIMBAD

6)Simulation

7)Exécution

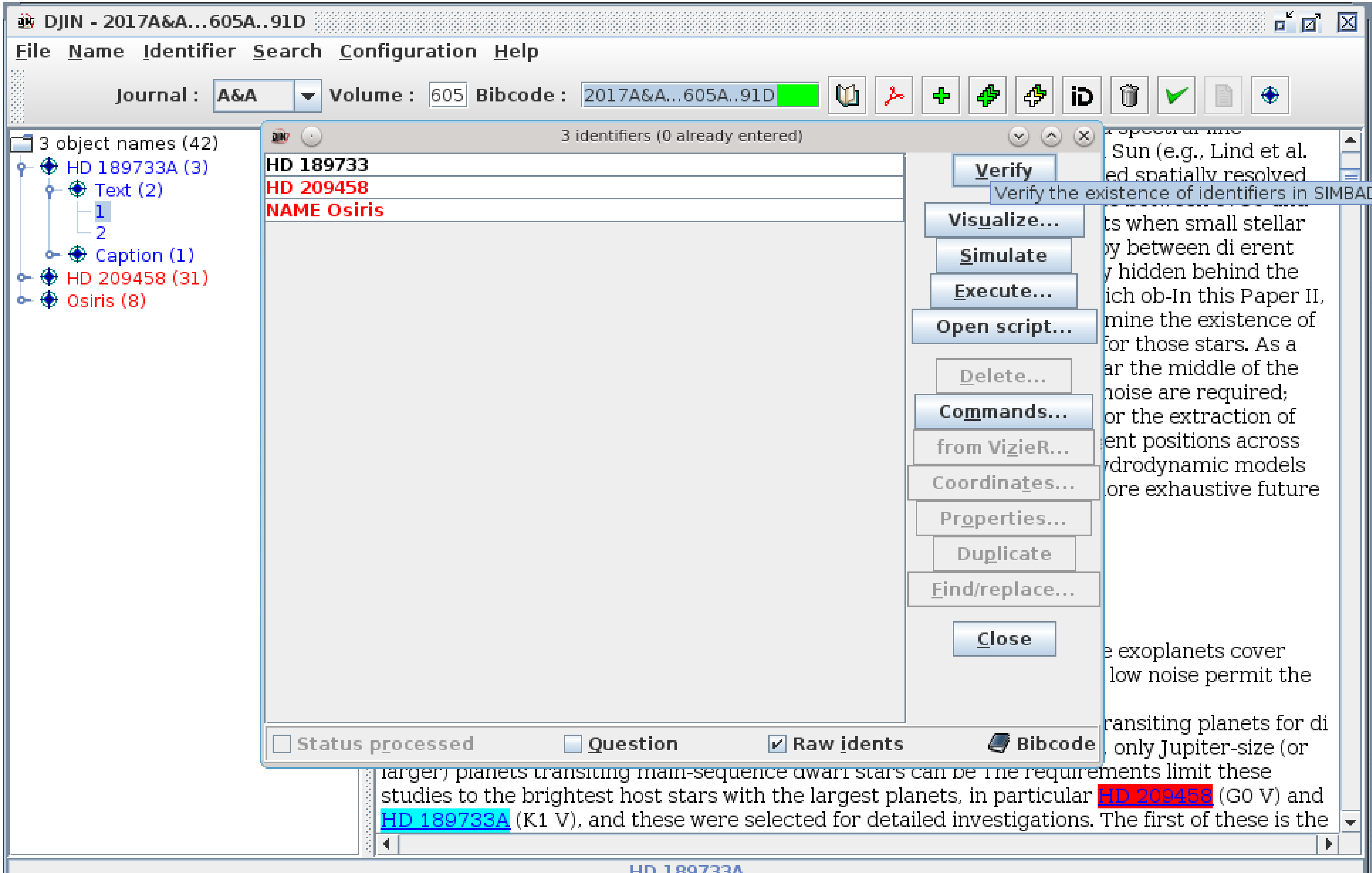
DJIN - 2017A&A...605A..91D
File Name Identifier Search Configuration Help
Journal : A&A
Volume : 605
Bibcode : 2017A&A...605A..91D
3 object names (42)
HD 189733A (3)
Text (2)
1
2
Caption (1)
HD 209458 (31)
Osiris (8)
3 identifiers (0 already entered)
HD 189733
HD 209458
NAME Osiris
Verify
Verify the existence of identifiers in SIMBAD
Visualize...
Simulate
Execute...
Open script...
Delete...
Commands...
from VizieR...
Coordinates...
Properties...
Duplicate
Find/replace...
Close
Status processed
Question
Raw idents
Bibcode
Sun (e.g., Lind et al.
ed spatially resolved
ts when small stellar
py between di erent
y hidden behind the
ich ob-In this Paper II,
mine the existence of
for those stars. As a
ar the middle of the
noise are required;
or the extraction of
ent positions across
ydrodynamic models
ore exhaustive future
e exoplanets cover
low noise permit the
ransiting planets for di
only Jupiter-size (or
studies to the brightest host stars with the largest planets, in particular HD 209458 (G0 V) and
HD 189733A (K1 V), and these were selected for detailed investigations. The first of these is the
HD 189733A

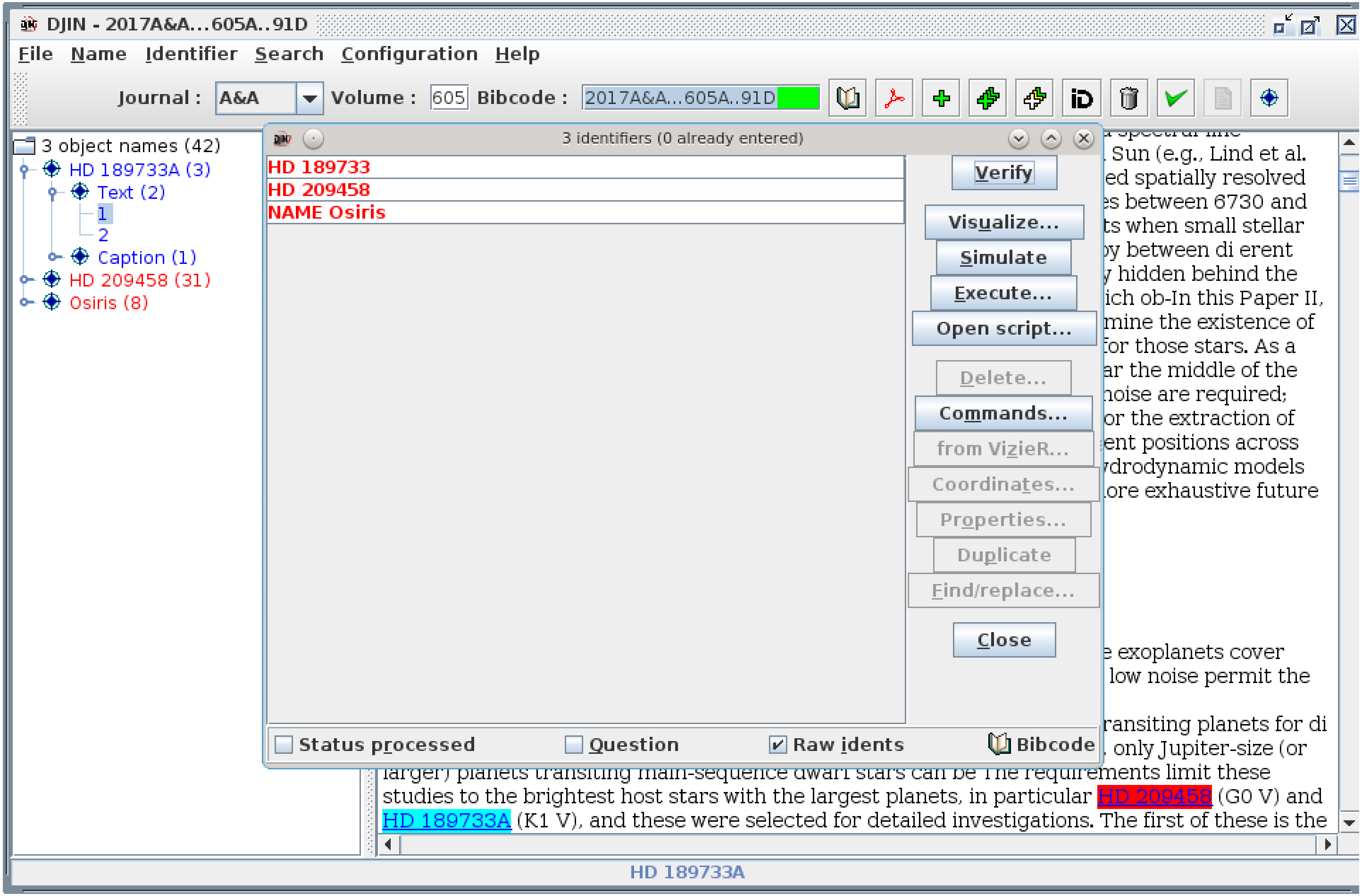
DJIN - 2017A&A...605A..91D
File Name Identifier Search Configuration Help
Journal : A&A Volume : 605 Bibcode : 2017A&A...605A..91D
3 object names (42)
HD 189733A (3)
Text (2)
1
2
Caption (1)
HD 209458 (31)
Osiris (8)
3 identifiers (0 already entered)
HD 189733
HD 209458
NAME Osiris
Verify
Visualize...
Simulate
Execute...
Open script...
Delete...
Commands...
from VizieR...
Coordinates...
Properties...
Duplicate
Find/replace...
Close
Status processed
Question
Raw idents
Bibcode
studies to the brightest host stars with the largest planets, in particular HD 209458 (G0 V) and
HD 189733A (K1 V), and these were selected for detailed investigations. The first of these is the
HD 189733A

TRAITER UN ARTICLE

1) Ouvrir avec DJIN

2)Eliminer le bruit

3)Lecture de l'article en diagonale

4)Identification des objets restants

5)Verify

6)Simulation
Permet de visualiser le script et ses éventuels bugs

7)Exécution

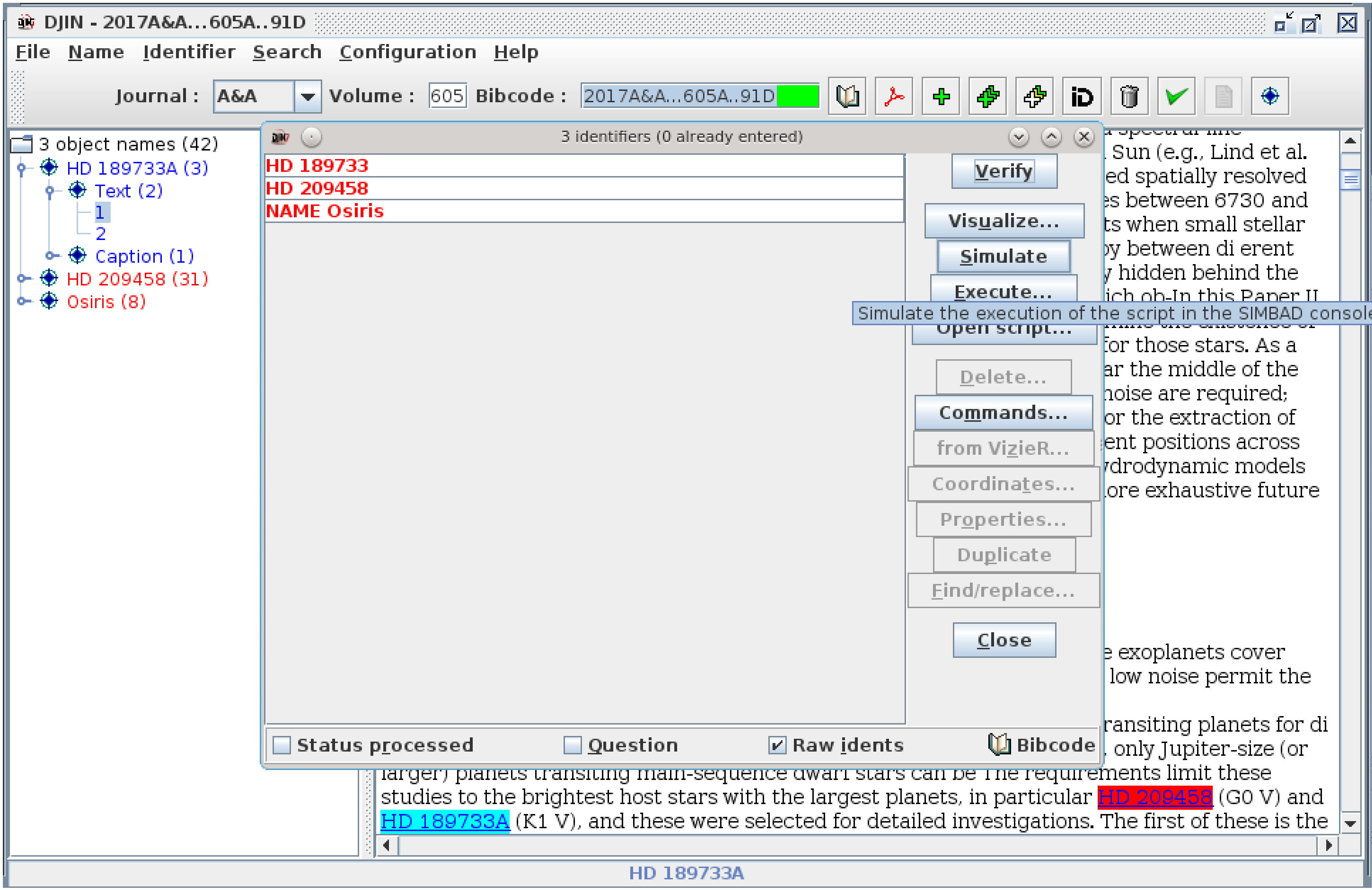
DJIN - 2017A&A...605A..91D
File Name Identifier Search Configuration Help
Journal : A&A Volume : 605 Bibcode : 2017A&A...605A..91D
3 object names (42)
HD 189733A (3)
Text (2)
1
2
Caption (1)
HD 209458 (31)
Osiris (8)
3 identifiers (0 already entered)
HD 189733
HD 209458
NAME Osiris
Verify
Visualize...
Simulate
Execute...
Simulate the execution of the script in the SIMBAD console
Open script...
Delete...
Commands...
from VizieR...
Coordinates...
Properties...
Duplicate
Find/replace...
Close
Status processed
Question
Raw idents
Bibcode
studies to the brightest host stars with the largest planets, in particular HD 209458 (G0 V) and
HD 189733A (K1 V), and these were selected for detailed investigations. The first of these is the
HD 189733A

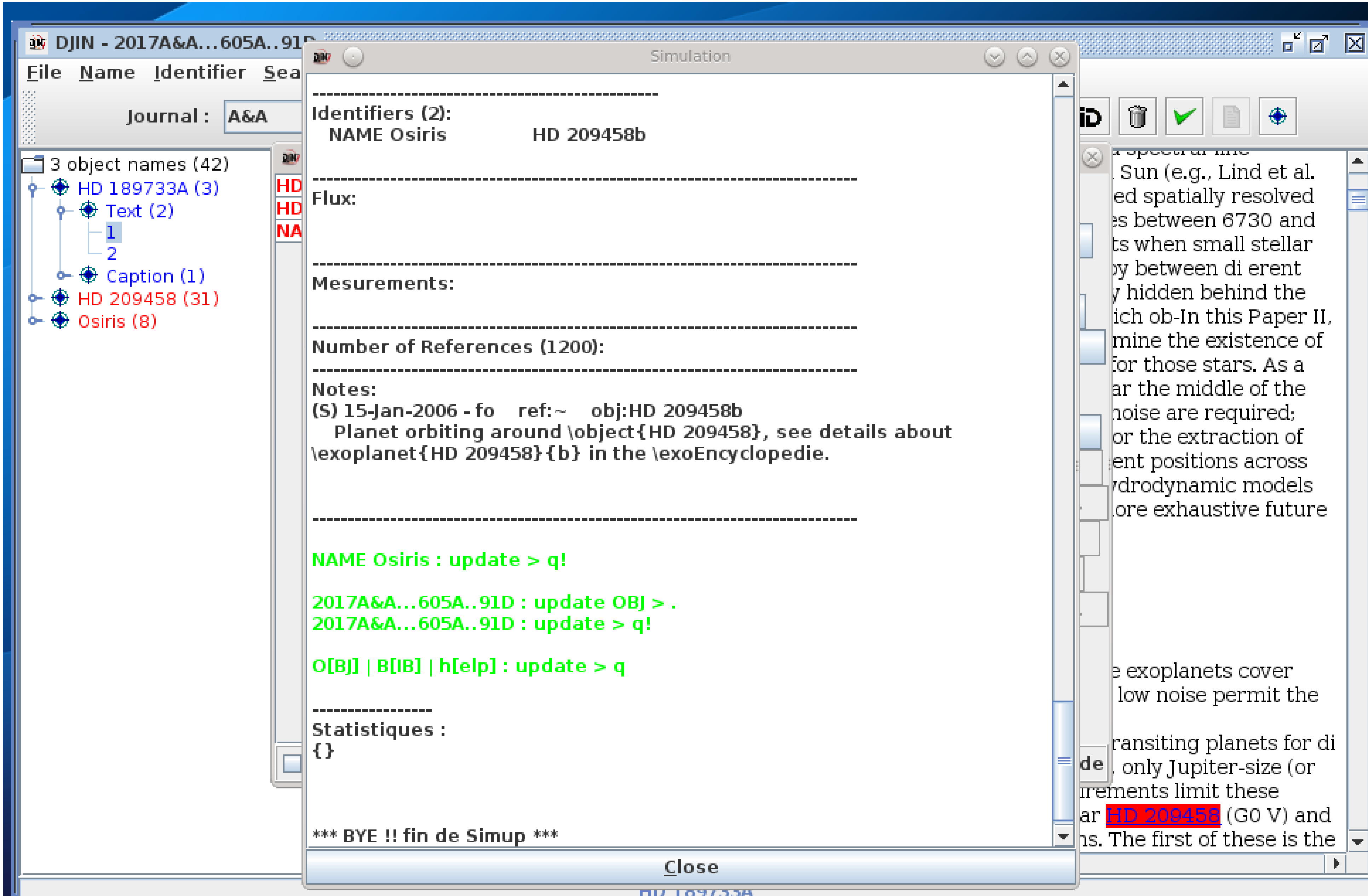
DJIN - 2017A&A...605A..91D
File Name Identifier Sea
Journal : A&A
3 object names (42)
HD 189733A (3)
Text (2)
1
2
Caption (1)
HD 209458 (31)
Osiris (8)
Simulation
Identifiers (2):
NAME Osiris HD 209458b
Flux:
Mesurements:
Number of References (1200):
Notes:
(S) 15-Jan-2006 - fo ref:~ obj:HD 209458b
Planet orbiting around \object{HD 209458}, see details about \exoplanet{HD 209458}{b} in the \exoEncyclopedie.
NAME Osiris : update > q!
2017A&A...605A..91D : update OBJ > .
2017A&A...605A..91D : update > q!
O[BJ] | B[IB] | h[elp] : update > q
Statistiques :
{}
*** BYE !! fin de Simup ***
Close
HD 209458 (G0 V) and

TRAITER UN ARTICLE

1) Ouvrir avec DJIN

2)Eliminer le bruit

3)Lecture de l'article en diagonale

4)Identification des objets restants

5)Verify

6)Simulation

7)Exécution

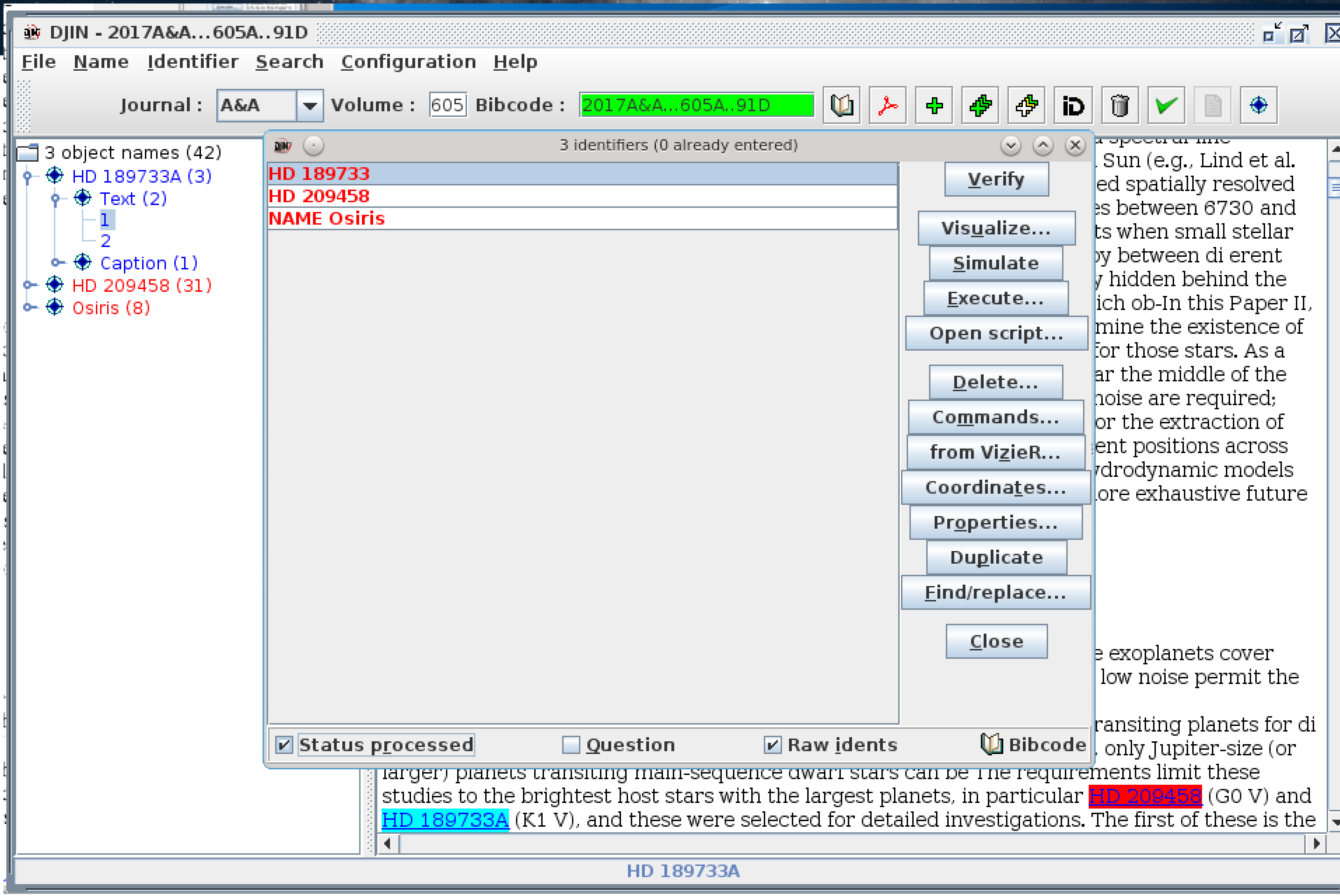
DJIN - 2017A&A...605A..91D
File Name Identifier Search Configuration Help
Journal : A&A Volume : 605 Bibcode : 2017A&A...605A..91D
3 object names (42)
HD 189733A (3)
Text (2)
1
2
Caption (1)
HD 209458 (31)
Osiris (8)
3 identifiers (0 already entered)
HD 189733
HD 209458
NAME Osiris
Verify
Visualize...
Simulate
Execute...
Open script...
Delete...
Commands...
from VizieR...
Coordinates...
Properties...
Duplicate
Find/replace...
Close
Status processed
Question
Raw idents
Bibcode
studies to the brightest host stars with the largest planets, in particular HD 209458 (G0 V) and
HD 189733A (K1 V), and these were selected for detailed investigations. The first of these is the
HD 189733A

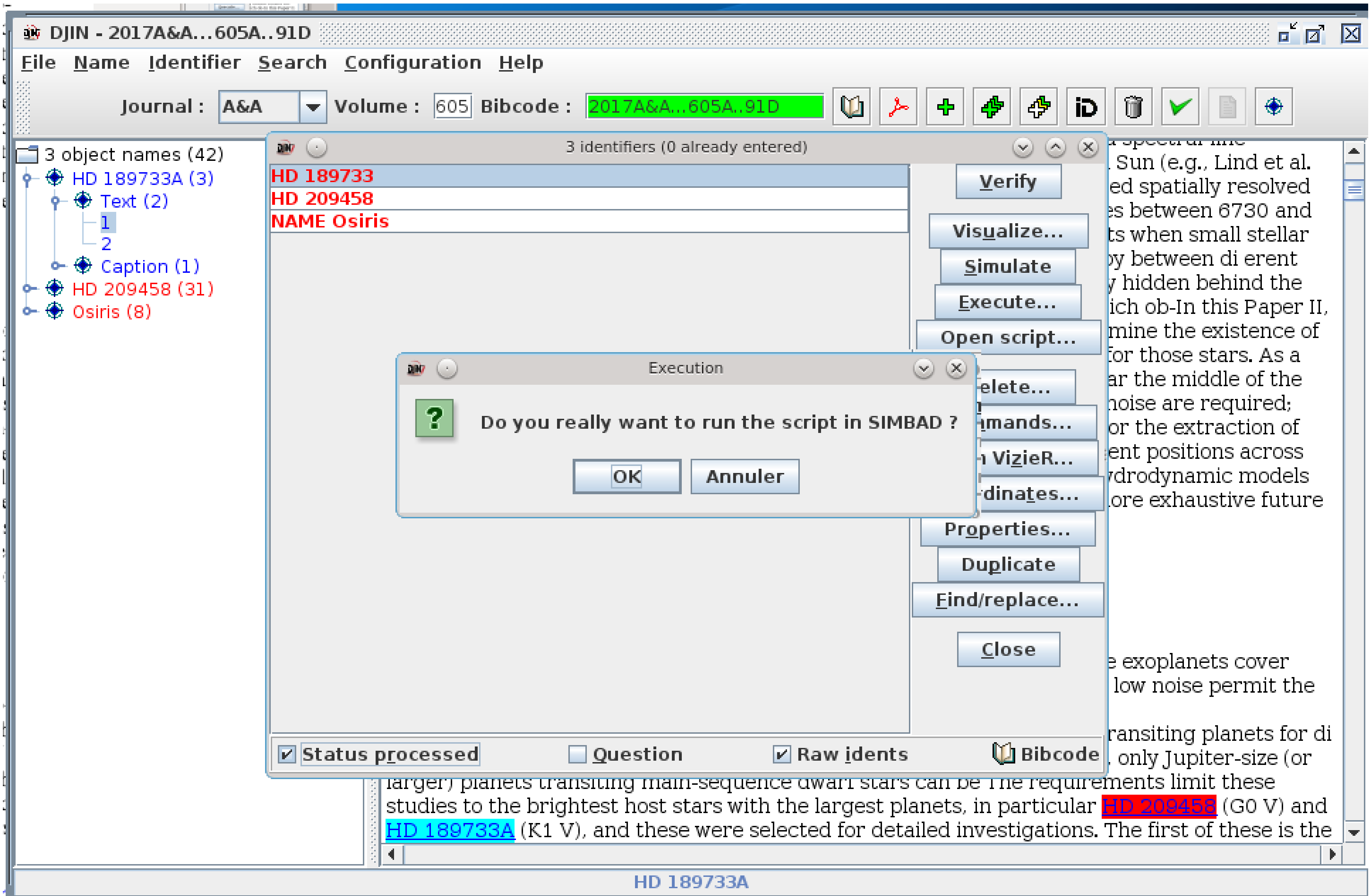
DJIN - 2017A&A...605A..91D
File Name Identifier Search Configuration Help
Journal : A&A Volume : 605 Bibcode : 2017A&A...605A..91D
3 object names (42)
HD 189733A (3)
Text (2)
1
2
Caption (1)
HD 209458 (31)
Osiris (8)
3 identifiers (0 already entered)
HD 189733
HD 209458
NAME Osiris
Verify
Visualize...
Simulate
Execute...
Open script...
Properties...
Duplicate
Find/replace...
Close
Execution
Do you really want to run the script in SIMBAD ?
OK
Annuler
Status processed
Question
Raw idents
Bibcode
studies to the brightest host stars with the largest planets, in particular HD 209458 (G0 V) and
HD 189733A (K1 V), and these were selected for detailed investigations. The first of these is the
HD 189733A

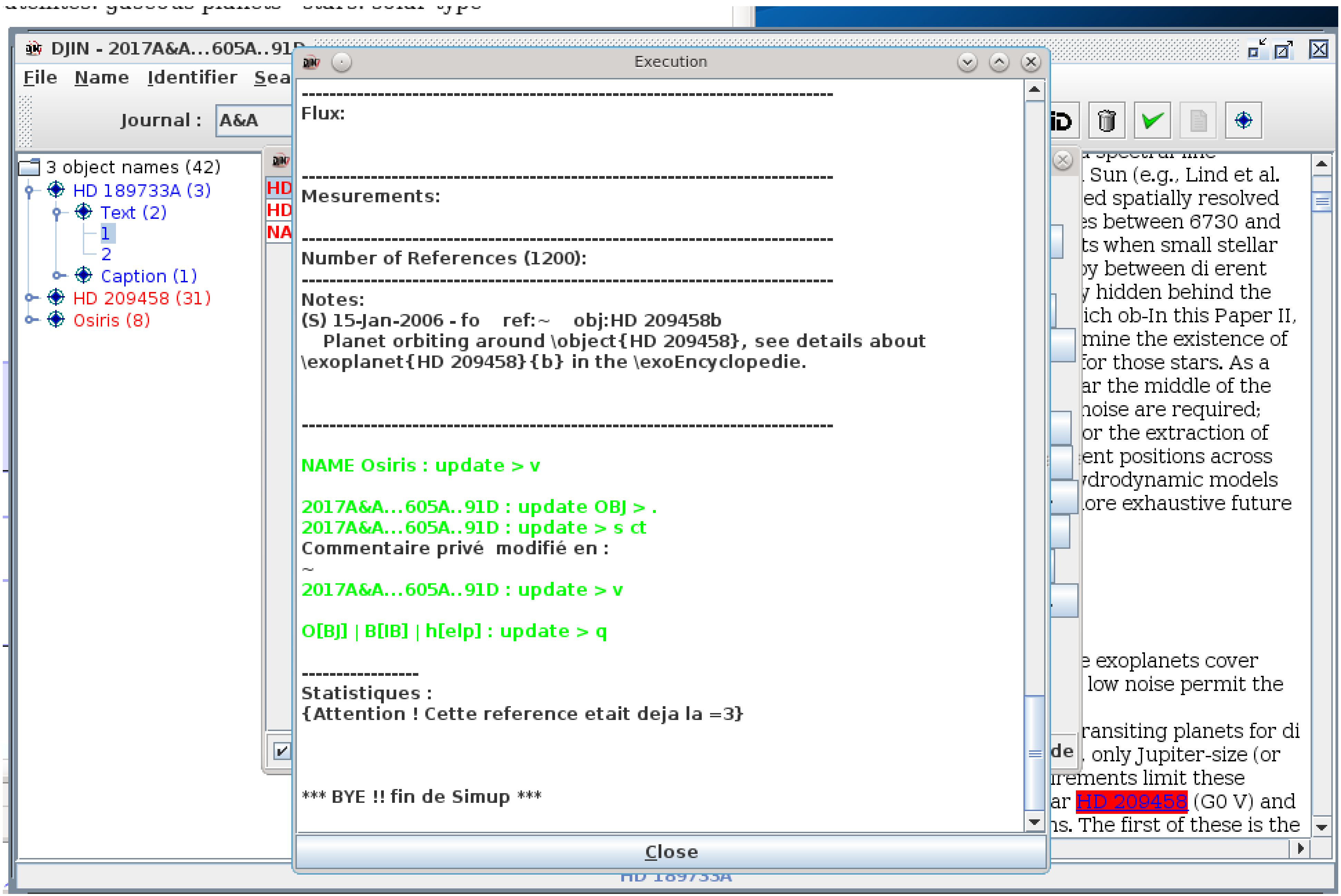
DJIN - 2017A&A...605A..91D
File Name Identifier Sea
Journal : A&A
3 object names (42)
HD 189733A (3)
Text (2)
1
2
Caption (1)
HD 209458 (31)
Osiris (8)
Execution
Flux:
Mesurements:
Number of References (1200):
Notes:
(S) 15-Jan-2006 - fo ref:~ obj:HD 209458b
Planet orbiting around \object{HD 209458}, see details about
\exoplanet{HD 209458}{b} in the \exoEncyclopedie.
NAME Osiris : update > v
2017A&A...605A..91D : update OBJ > .
2017A&A...605A..91D : update > s ct
Commentaire privé modifié en :
~
2017A&A...605A..91D : update > v
O[BJ] | B[IB] | h[elp] : update > q
Statistiques :
{Attention ! Cette reference etait deja la =3}
*** BYE !! fin de Simup ***
Close
HD 209458 (G0 V) and

2017A&A...605A..91D - *Astron. Astrophys., 605A, 91-91 (2017) - 23.10.17 23.10.17 September(I) 2017 2017-09-15*

Spatially resolved spectroscopy across stellar surfaces. II. High-resolution spectra across HD 209458 (G0 V).

DRAVINS D.; LUDWIG H.-G.; DAHLEN E.; PAZIRA H.

Abstract (from CDS): Context. High-resolution spectroscopy across spatially resolved stellar surfaces aims at obtaining spectral-line profiles that are free from rotational broadening; the gradual changes of these profiles from disk center toward the stellar limb reveal properties of atmospheric fine structure, which are possible to model with 3D hydrodynamics. Aims. Previous such studies have only been carried out for the Sun but are now extended to other stars. In this work, profiles of photospheric spectral lines are retrieved across the disk of the planet-hosting star HD 209458 (G0 V). Methods. During exoplanet transit, stellar surface portions successively become hidden and differential spectroscopy provides spectra of small surface segments temporarily hidden behind the planet. The method was elaborated in Paper I (Dravins et al., 2017A&A...605A..90D), with observable signatures quantitatively predicted from hydrodynamic simulations. Results. From observations of HD 209458 with spectral resolution λ/Δλ~80000, photospheric FeI line profiles are obtained at several center-to-limb positions, reaching adequately high S/N after averaging over numerous similar lines. Conclusions. Retrieved line profiles are compared to synthetic line profiles. Hydrodynamic 3D models predict, and current observations confirm, that photospheric absorption lines become broader and shallower toward the stellar limb, reflecting that horizontal velocities in stellar granulation are greater than vertical velocities. Additional types of 3D signatures will become observable with the highest resolution spectrometers at large telescopes.

Journal keyword(s): stars: atmospheres - techniques: spectroscopic - line: profiles - hydrodynamics - planets and satellites: gaseous planets - stars: solar-type

Simbad objects: 3

▸ Full paper

▸ View the reference in ADS

Number of rows : 3 Plot

Show 100 entries

N	Identifier	obj tags	obj count	Otype	ICRS (J2000) RA	ICRS (J2000) DEC	Mag U	Mag B	Mag V
1	HD 189733	*cx*	*3*	BY*	20 00 43.7128	+22 42 39.074	9.241	8.578	7.648
2	NAME Osiris	*sx*	*8*	Pl	22 03 10.77207	+18 53 03.5430			
3	V* V376 Peg	*tascx*	*31*	EP*	22 03 10.7728	+18 53 03.550		8.21	7.63

Showing 1 to 3 of 3 entries

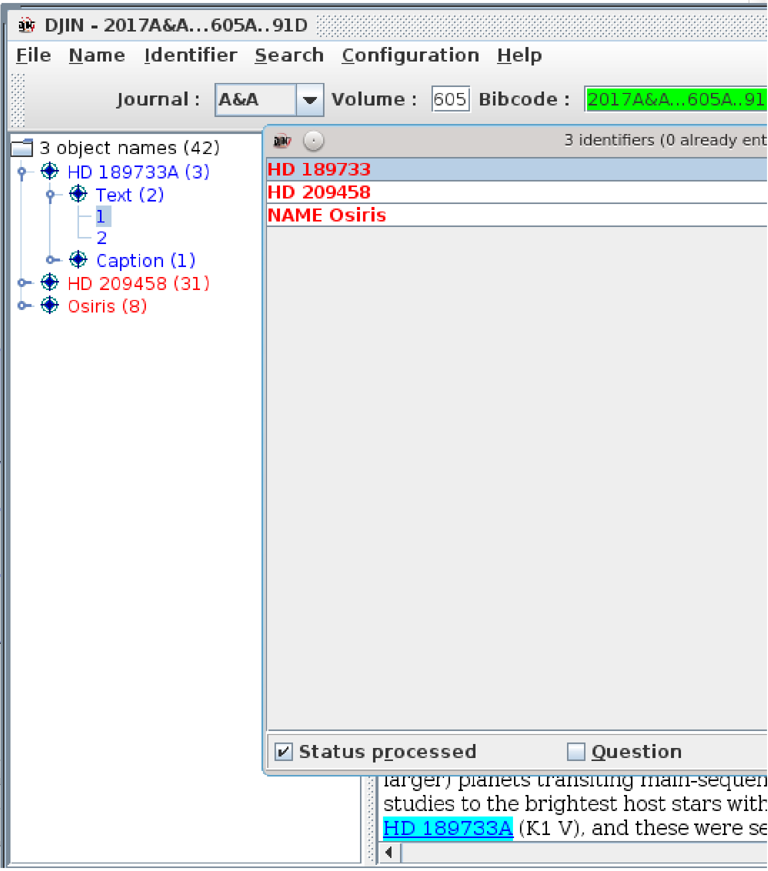

3 pièces jointes 219 Ko

The spectroscopically observed profiles are different from each from the measured Rossiter-McLaughlin effect.

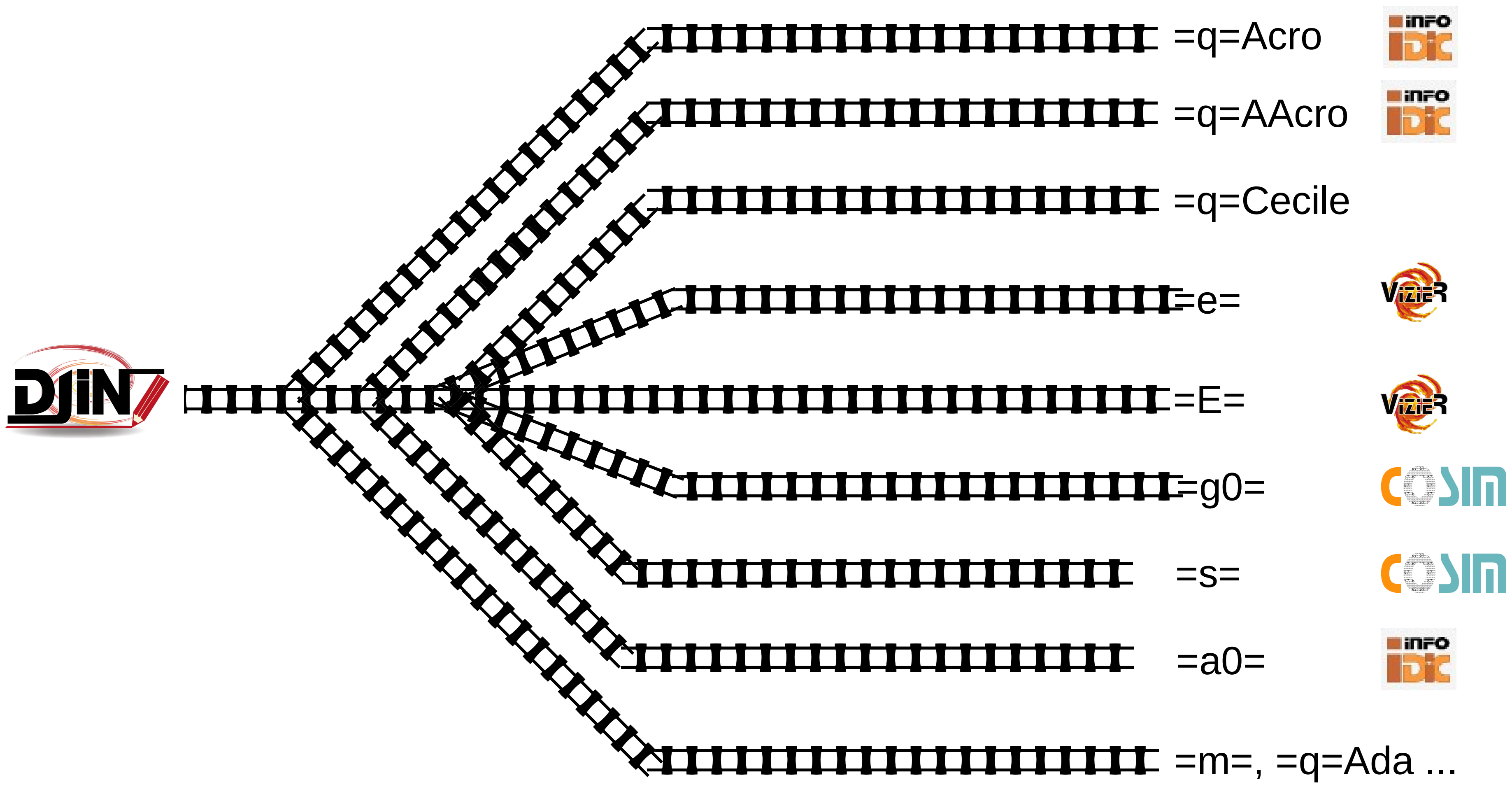

=q=Acro
=q=AAcro
=q=Cecile
=e=
=E=
=g0=
=s=
=a0=
=m=, =q=Ada ...

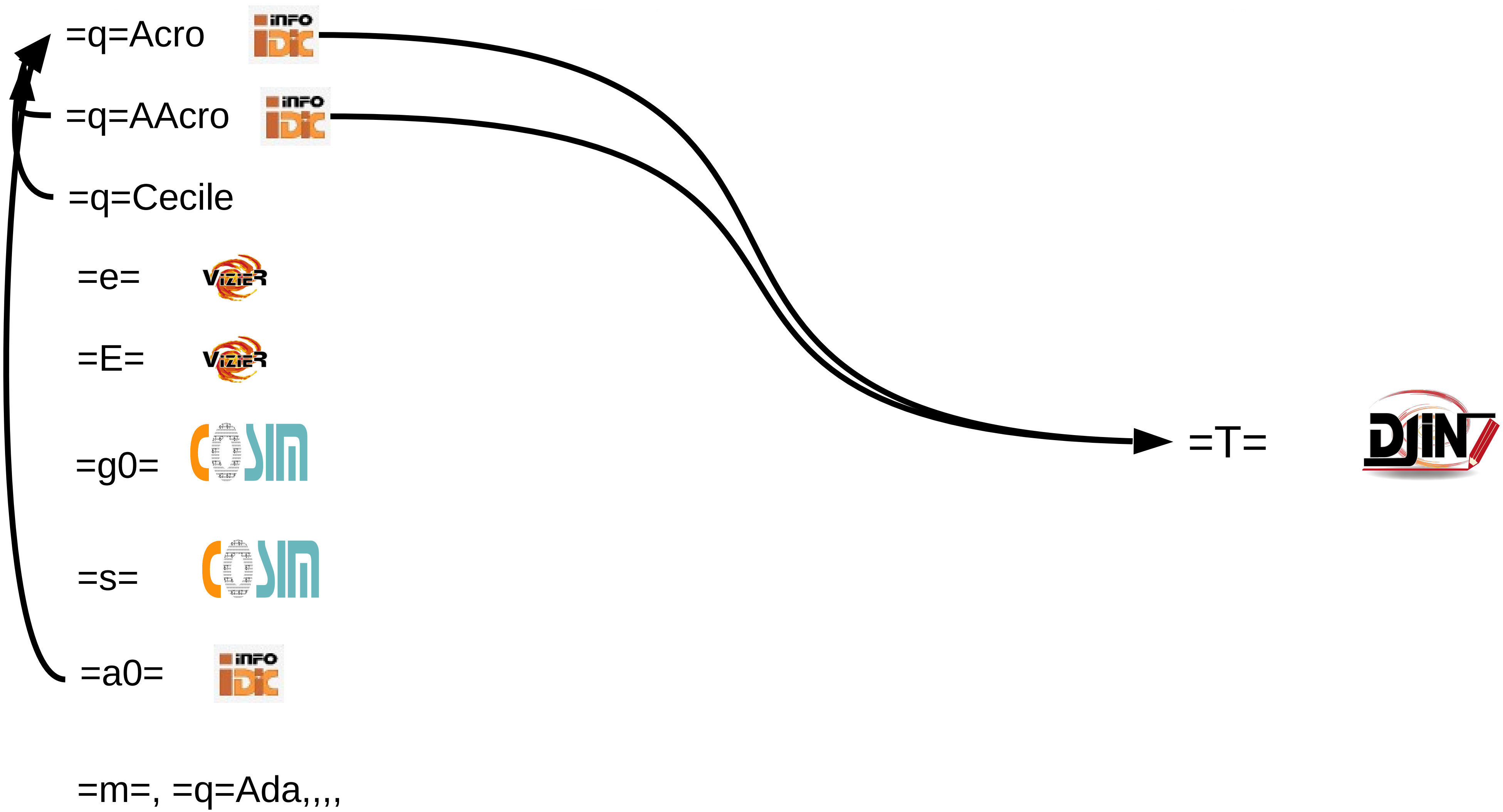

=q=Acro
=q=AAcro
=q=Cecile
=e=
=E=
=g0=
=s=
=a0=
=m=, =q=Ada,,,,
=T=

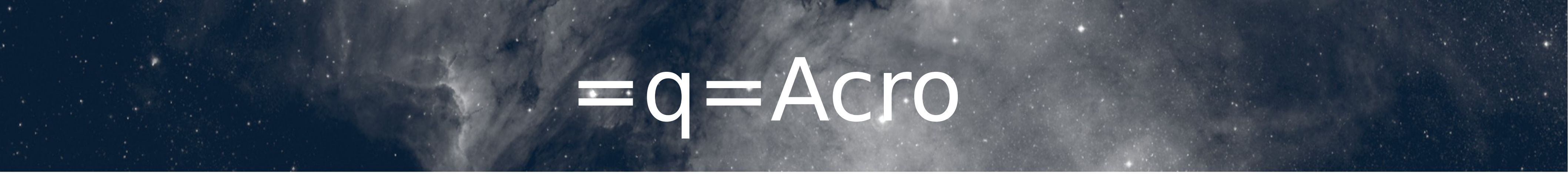

Appendix A: Optical identifications

In this Appendix we report the full list of optical counterparts belonging to A 2142 in the same field shown in Fig. 2, and radio/optical overlays both for the extended radio galaxies and for those groups where multiple radio emission has been detected.

Table A.1. Optical identifications with cluster galaxies.

#, GMRT name	α_{J2000} radio	δ_{J2000} radio	$S_{608\ MHz}$ (mJy)	$S_{234\ MHz}$ (mJy)	log $P_{608\ MHz}$(W/Hz)	Notes
Optical Catalogue	α_{J2000} opt	δ_{J2000} opt	m_g		z	
#1, GMRT-J 155636+270041	15 56 36.99	27 00 41.7	1.67	6.52	22.55	P
WISEPC	15 56 37.07	27 00 39.7	15.9		0.091117	
#2, GMRT-J 155642+273324	15 56 42.94	27 33 24.1	3.18	5.71	22.80	P
2MASX	15 56 42.96	27 33 24.6	17.0		0.088777	
#3, GMRT-J 155646+270015	15 56 46.20	27 00 15.2	0.53	–	21.99	P
SDSS	15 56 46.25	27 00 15.4	18.9		0.085227	
#4, GMRT-J 155700+273102	15 57 00.56	27 31 02.2	1.87	4.42	22.50	P
2MASX	15 57 00.56	27 31 02.7	17.8		0.082248	
#5, GMRT-J 155703+271812	15 57 03.29	27 18 12.8	1.53	3.65	22.54	P
2MASX	15 57 03.34	27 18 12.7	16.8		0.094222	

=q=AAcro

also the images in the MOJAVE webpage).

The disappearance of strong IDV in S4 0917+624 after the year 2000 cannot be fully explained with the quenching mechanism via changes of core size in the source, as discussed above. Bernhart et al. (2006) studied the VLBI kinematics of S4 0917+624 with data during 2000–2007 at 5, 15, and 22 GHz, and also did not find clear correlation between the IDV properties and VLBI structure. The disappearance is likely caused by a change of ISM scattering properties, e.g. with the passage of scattering material out of the line of sight to the quasar, as discussed for the fast IDV source J1819+3845, which also ceased at some time in the period between June 2006 and February 2007 (de Bruyn & Macquart 2015), and for the intermittent IDV source PKS 0405–385 (Kedziora-Chudczer 2006).

To identify the possible scattering materials located in the foreground of S4 0917+624, which has the distance ~200 pc estimated with the shortest timescale in the appendix by Rickett

=q=Cecile

Table 1. Detected sources.

Source ID	RA	Dec	Size (arcsec × arsec)	Reference
Map M1/Band 3				
1a	07:47:30.817	–19:17:18.48	1.76″ × 1.57″	USNO B1.0 0707-10151219
2a	07:47:30.520	–19:17:23.39	2.01″ × 1.85″	unknown
Bright source in Fig. 10b	17:47:30.130	–19:17:50.60	2.56″ × 2.42″	2MASX J07473002-1917503
Map M2/Band 7				
1b	07:47:31.206	–19:17:37.38	0.32″ × 0.26″	unknown
2b	07:47:31.642	–19:17:38.85	0.52″ × 0.40″	unknown
3b	07:47:31.228	–19:17:37.35	0.35″ × 0.34″	unknown
1b+3b (as a single source)	07:47:31.220	–19:17:37.35	0.44″ × 0.32″	unknown
4b	07:47:30.982	–19:17:36.53	0.34″ × 0.24″	unknown
Map M3/Band 3 + Band 7				
1c	07:47:31.618	–19:17:35.464	0.39″ × 0.18″	unknown
2c	07:47:30.974	–19:17:35.464	0.41″ × 0.24″	unknown
3c	07:47:31.192	–19:17:37.33	0.57″ × 0.31″	same as 1b+3b in M2

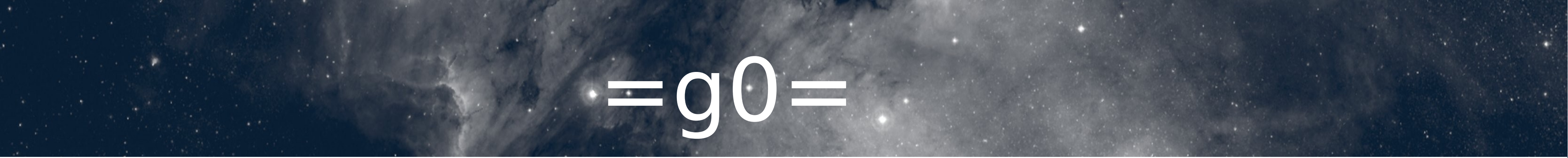

Table 1. Stars considered for this paper, including information about line broadening, stellar parameters, and the quantity *RS k* (relative skewness, see Eq. (1)).

Target	SpC	Line	S/N_c	EW	$v \sin i$		v_{mac}	$RS\,k$	σ_{RSk}	$\log T_{eff}$	$\log \mathscr{L}/\mathscr{L}_\odot$
					FT	GOF	GOF				
...	...	...	...	...	...	...	...	...	...	...	...
HD 16582	B2 IV	Si III	183	138	9	9	19	0.02	0.05	4.34	2.94
HD 17081	B7 V	Mg II	195	294	18	19	24	−0.03	0.02	4.12	2.40
HD 17603	O7.5 Ib(f)	O III	239	317	109	99	115	−0.01	0.02	4.53	4.21
HD 17743	B8 III	Mg II	157	214	48	47	22	0.00	0.06	4.13	2.21
HD 18409	O9.7 Ib	O III	256	179	131	128	<88	0.08	0.16	4.51	3.99
HD 18604	B6 III	Mg II	184	305	131	132	<50	0.07	0.08	4.11	2.44
HD 19820	O8.5 III(n)((f))	O III	316	251	144	147	<54	−0.22	0.11	4.51	3.91
...	...	...	...	...	...	...	...	...	...	...	...

Notes. The line used to determine the line-broadening parameters is also indicated, along with its equivalent width and the signal-to-noise ratio of the adjacent continuum. Spectral classifications indicated in Col. 2 must be handled with caution since they come from various sources, not all of which are equally reliable. EW in mÅ, $v \sin i$ and v_{mac} in km s^{-1}, T_{eff} in K. The full table is available at the CDS.

* Full Table 1 is only available at the CDS via anonymous ftp to cdsarc.u-strasbg.fr (130.79.128.5) or via http://cdsarc.u-strasbg.fr/viz-bin/qcat?J/A+A/597/A22

[1] Throughout this paper, and following Reed (2003), we use the term OB stars to refer to O- and early-B type stars on the main sequence and their evolved descendants, the B supergiants. The remaining B-type stars (dwarfs and giants) are considered as a separate group.

the
bro
tech
fitti
pro
the

Article publishec

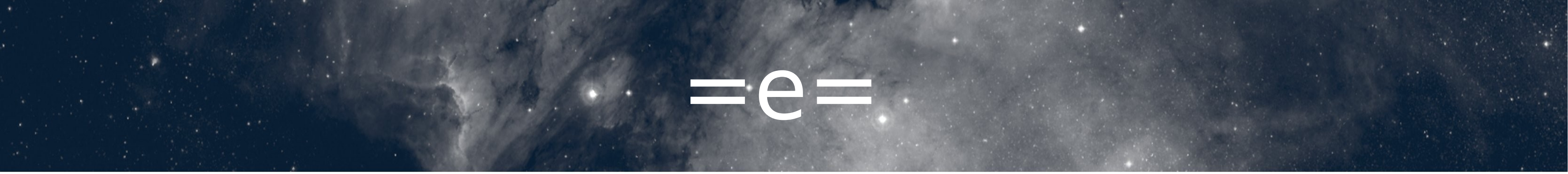

Table 1
Data on the *Fermi*/LAT Blazar Candidates (583 Sources)

LAT Name	Counterpart Name	Class	$\log \nu_s$	Γ_γ	$\alpha_{r\gamma}$	α_{rx}	α_{ox}	ρ_s^1	ρ_s^2	ρ_s^3	IT
J2250.3−4206	PMN J2250−4206	BCU I	13.92	2.034	0.750	⋯	⋯	0.45	⋯	⋯	⋯
J1647.4+4950	SBS 1646+499	BCU I	13.68	2.429	0.759	0.662	1.693	−0.20	−0.38	0.10	Q
J1412.0+5249	SBS 1410+530	BCU I	15.364	2.562	0.875	0.776	2.181	−0.90	−0.88	−0.41	⋯
J0343.3+3622	OE 367	BCU I	12.28	2.426	0.828	⋯	⋯	−0.73	⋯	⋯	Q
J0647.6−6058	PMN J0647−6058	BCU I	13.11	2.337	0.759	⋯	⋯	−0.07	⋯	⋯	⋯
J0040.5−2339	PMN J0040−2340	BCU I	14.358	1.946	0.768	⋯	⋯	0.40	⋯	⋯	⋯
J2040.2−7115	PKS 2035−714	BCU I	16.15	1.798	0.795	0.624	⋯	0.32	0.49	⋯	⋯
J0151.0−3609	PMN J0151−3605	BCU I	⋯	2.459	0.772	⋯	⋯	−0.35	⋯	⋯	⋯
J2336.5+2356	B2 2334+23	BCU I	⋯	2.134	0.822	0.639	⋯	−0.24	0.09	⋯	⋯
J0132.5−0802	PKS 0130−083	BCU I	15.75	1.753	0.807	0.632	1.409	0.28	0.49	−0.31	⋯
J0618.9−1138	TXS 0616−116	BCU I	13.75	2.470	0.822	⋯	⋯	−0.75	⋯	⋯	⋯
J1416.0+1325	PKS B1413+135	BCU I	12.865	2.363	0.843	⋯	⋯	−0.68	⋯	⋯	⋯
J0059.1−5701	PKS 0056−572	BCU I	12.77	2.616	0.827	0.682	1.004	−0.87	−0.64	−0.70	⋯
J0749.4+1059	TXS 0746+110	BCU I	14.265	2.203	0.795	⋯	⋯	−0.16	⋯	⋯	⋯
J1604.4−4442	PMN J1604−4441	BCU I	12.947	2.453	0.793	⋯	⋯	−0.50	⋯	⋯	⋯

Table 8
List of New Minimum Timings Used for the Analysis

Star	JD Hel.-2400000	Error (day)	Type	Filter	Source/Observatory
V773 Cas	48500.8874	0.0095	Prim	Hp	*Hipparcos*
V773 Cas	54798.48508	0.00154	Prim	BVR	PS—this study
V773 Cas	55062.39534	0.00139	Prim	BVR	PS—this study
V773 Cas	55071.45118	0.00133	Prim	BVR	PS—this study
V773 Cas	55410.39017	0.00197	Prim	BVR	PS—this study
V773 Cas	55419.44651	0.00101	Prim	BVR	PS—this study
V773 Cas	55481.54064	0.00182	Prim	BVR	PS—this study
V773 Cas	55754.50689	0.00038	Sec	I	RU—this study
V773 Cas	55776.49780	0.00026	Prim	R	PS—this study
V773 Cas	55776.49748	0.00066	Prim	I	RU—this study
V773 Cas	55877.40172	0.00047	Prim	R	RU—this study
V773 Cas	56155.54350	0.00069	Sec	R	RU—this study
V773 Cas	56159.42162	0.00105	Prim	R	RU—this study
V773 Cas	56230.57514	0.00062	Sec	C	RU—this study
V773 Cas	56252.56717	0.00075	Prim	C	RU—this study
V773 Cas	56304.31383	0.00040	Prim	C	RU—this study
V773 Cas	56516.47530	0.00062	Prim	I	RU—this study
V773 Cas	56538.46837	0.00084	Sec	C	RU—this study

Table 2. Sources in the clean sample.

(1) ID_{VUDS}	(2) ID_{HST}	(3) RA (deg)	(4) Dec (deg)	(5) z_{spec}	(6) Flag	(7) V (mag)	(8) $f_\lambda(895)$ (10^{-19})	(9) err $f_\lambda(895)$ (10^{-19})	(10) $f_\lambda(1470)$ (10^{-19})	(11) err $f_\lambda(1470)$ (10^{-19})	(12) $EW_{Ly\alpha}$ (Å)
	COSMOS/CANDELS										
510998698	6772	150.082313	2.261036	4.0651	9	25.83 ± 0.12	1.98	3.23	9.04	1.49	–24.99
511002138	4913	150.122450	2.237101	4.3600	9	24.90 ± 0.06	8.25	3.26	17.08	5.63	–19.18
511227001	20282	150.062182	2.423024	3.6350	3	25.57 ± 0.11	1.79	1.39	9.26	0.48	–23.84
5100998496	6868	150.205055	2.262162	3.8979	4	25.90 ± 0.15	–3.93	1.68	17.24	0.60	≥0
5101226001	20579	150.189291	2.427818	3.7327	3	25.71 ± 0.11	1.39	2.10	11.70	0.46	≥0
5101226251	20598	150.157203	2.42786	3.9888	3	25.42 ± 0.10	–4.95	1.40	17.74	0.52	≥0
5101233433*	16703	150.186851	2.379107	3.7403	4	25.19 ± 0.08	5.35	1.64	18.72	0.38	≥0
5101233724	16397	150.177453	2.375223	4.3862	4	26.51 ± 0.20	–1.73	1.55	9.55	0.56	–11.11
5101242274	11634	150.191107	2.317958	4.3771	4	25.95 ± 0.16	–0.34	0.80	19.61	0.67	≥0
	ECDFS/CANDELS										
530029038	3753	53.0792917	–27.8772595	4.4179	3	26.70 ± 0.19	1.27	2.41	14.79	0.56	≥0
530030313	4503	53.1132794	–27.8698754	3.5789	3	26.04 ± 0.09	3.83	3.87	10.62	0.61	≥0
530030325	4542	53.1090745	–27.8697555	3.7519	4	25.42 ± 0.06	–0.34	1.41	21.25	0.43	≥0
530032655	5955	53.0940950	–27.854974	3.7222	2	25.71 ± 0.07	–0.80	1.24	13.67	0.41	≥0
530036055	8312	53.2208728	–27.8334905	4.1608	3	25.36 ± 0.05	–1.29	1.21	27.90	0.85	≥0
530037593	9317	53.156571	–27.824343	3.5336	2	25.79 ± 0.08	–2.44	2.46	11.68	0.36	≥0
530047200	17081	53.0640040	–27.765834	3.5600	2	26.06 ± 0.09	6.36	14.9	16.27	1.49	≥0
530049753*	18915	53.2104941	–27.7502276	3.6055	4	25.81 ± 0.08	2.92	0.93	10.68	0.20	≥0
530049877	18722	53.0147863	–27.7517345	3.8245	3	25.75 ± 0.08	2.53	2.20	16.14	0.50	–8.43
530050023	19009	53.2048527	–27.7494405	3.6097	4	25.07 ± 0.04	–3.43	2.43	21.29	0.55	≥0
530051970	20286	53.1989481	–27.7379129	3.7983	4	24.91 ± 0.04	–1.20	1.87	26.33	0.79	–5.32
	ECDFS/GEMS										
530003871	958	53.196500	–28.036822	3.9022	3	26.23 ± 0.12	1.61	1.25	11.81	0.49	≥0
530004745	1087	53.204005	–28.03064	3.6447	3	26.24 ± 0.11	–3.48	2.8	12.27	0.66	–18.61

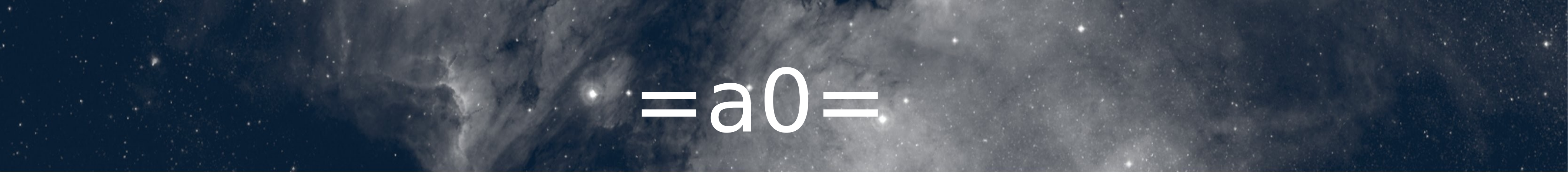

Table 1
Physical Properties of the *Herschel* Clumps Detected in Our Selected Field around I05480+2545 (see Figures 6(b) and (c))

ID	l (degree)	b (degree)	R_c (pc)	$M_{\rm clump}$ ($M_\odot$)
1	183.417	−0.607	1.6	545
2	183.390	−0.502	1.0	135
3	183.351	−0.537	1.1	240
4†	183.355	−0.580	1.7	1875
5	183.327	−0.514	0.8	105
6	183.273	−0.584	1.6	595
7	183.242	−0.623	0.8	90
8	183.215	−0.588	0.9	125
9	183.168	−0.603	0.9	130
10	183.117	−0.689	1.5	335
11	183.141	−0.786	1.6	385
12	183.203	−0.661	0.6	40
13	183.230	−0.755	0.4	15
14	183.110	−0.599	0.5	40
15	183.028	−0.693	0.5	35

Note. Column 1 gives the IDs assigned to the clump. The table also lists positions, deconvolved effective radius (R_c), and clump mass ($M_{\rm clump}$). The clump (ID No. 4) highlighted with a dagger contains a cluster of YSOs and the 6.7 GHz MME.

=m=

Table 1. List of BeSSeL sources observed with the JVLA.

Source	Position RA (J2000) (h m s)	Position Dec (J2000) (° ′ ″)	V_{LSR} (km s^{-1})	Dist. (kpc)	L_{bol} ($L_{\odot}$)
G000.67−0.04	17 47 20.1	−28 23 03	65.0	7.75 ± 0.72	7.3×10^5
G000.68−0.03	17 47 19.9	−28 22 19	55.0	7.75 ± 0.72	3.2×10^5
G005.88−0.39	18 00 30.3	−24 04 04	9	2.99 ± 0.18	5.8×10^4
G009.99−0.03	18 07 50.1	−20 18 56	50	*5.0*[a]	*1.2 × 10⁴*
G011.92−0.61	18 13 58.1	−18 54 20	30	3.37 ± 0.35	1.2×10^4
G012.43−1.12	18 16 52.1	−18 41 43	−30	*3.7*[a]	*4.2*[b] *× 10⁴*
G012.68−0.18	18 13 54.7	−18 01 47	59	2.40 ± 0.18	5.7×10^3
G012.90−0.24	18 14 34.4	−17 51 52	36	2.45 ± 0.15	8.6×10^2
G012.91−0.26	18 14 39.4	−17 52 06	41	2.53 ± 0.20	2.7×10^4
G014.64−0.58	18 19 15.5	−16 29 45	19	1.83 ± 0.07	1.1×10^3
G016.58−0.05	18 21 09.0	−14 31 49	64	3.58 ± 0.30	1.3×10^4
G024.49−0.04	18 36 05.7	−07 31 19	110	7.25[c] ± 1.42	3.8×10^4
G026.42+1.69	18 33 30.5	−05 01 02	55	*3.1*[a]	*9.0*[b] *× 10³*
G031.58+0.08	18 48 41.7	−01 09 59	96	4.90 ± 0.72	2.0×10^4
G035.02+0.35	18 54 00.7	+02 01 19	52	2.33 ± 0.22	1.0×10^4
G045.07+0.13	19 13 22.0	+10 50 53	59	8.00 ± 0.32	3.5×10^5
G048.61+0.02	19 20 31.2	+13 55 25	25	10.75 ± 0.58	2.8×10^5
G049.19−0.34	19 22 57.8	+14 16 10	67	5.29 ± 0.20	6.0×10^3
G074.04−1.71	20 25 07.1	+34 49 58	5	1.59 ± 0.05	*3.7*[b] *× 10²*
G075.76+0.34	20 21 41.1	+37 25 29	−10	3.51 ± 0.28	1.4×10^4
G076.38−0.62	20 27 25.5	+37 22 48	−2	1.30 ± 0.09	*1.4*[b] *× 10⁴*
G079.88+1.18	20 30 29.1	+41 15 54	−5	1.61 ± 0.07	8.6×10^2
G090.21+2.32	21 02 22.7	+50 03 08	−3	0.67 ± 0.02	2.7×10^1
G092.69+3.08	21 09 21.7	+52 22 37	−10	1.63 ± 0.05	(*4.7*[b] *× 10³*)

Quelques statistiques...

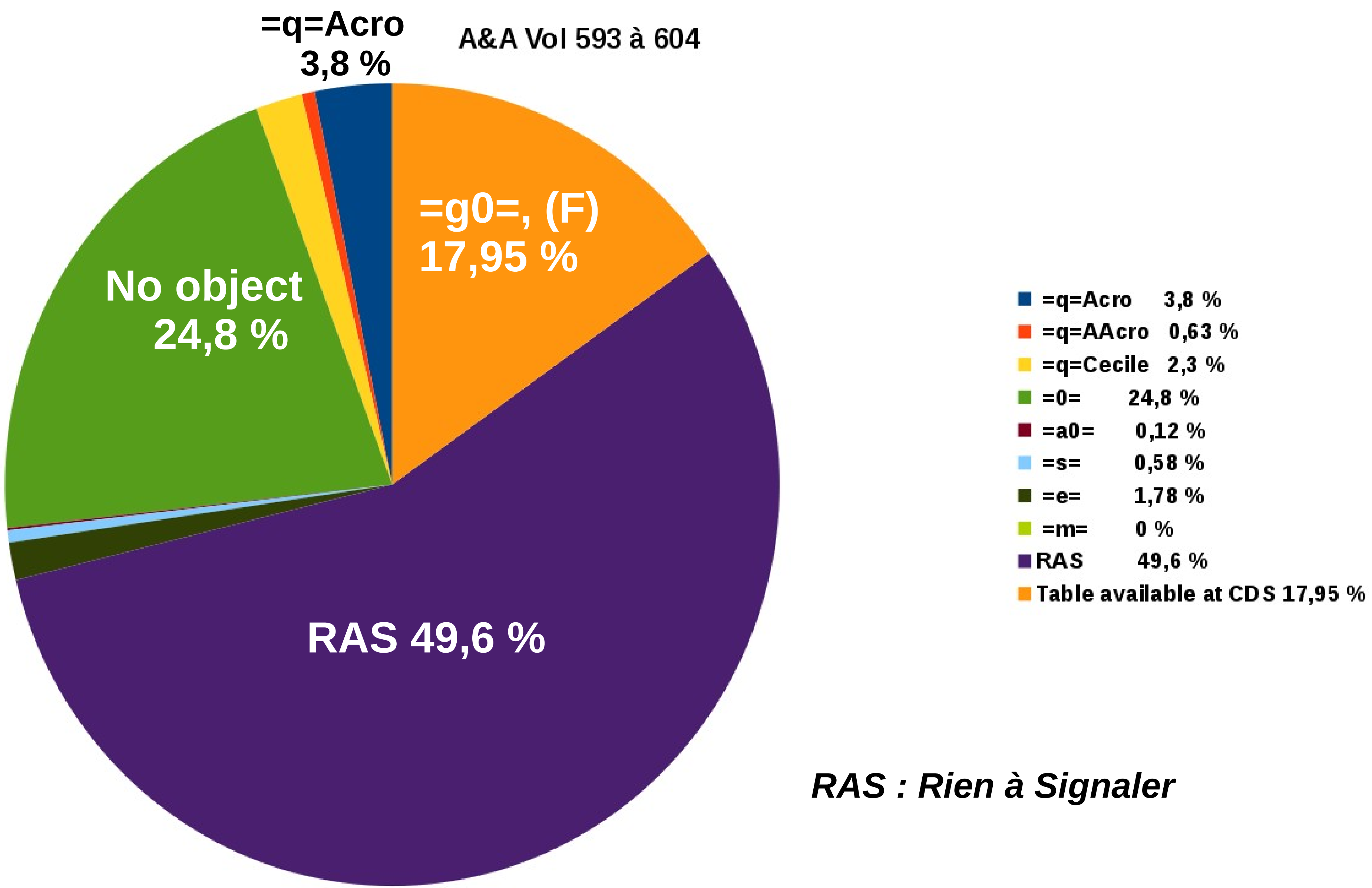

RAS : Rien à Signaler

Quelques statistiques...

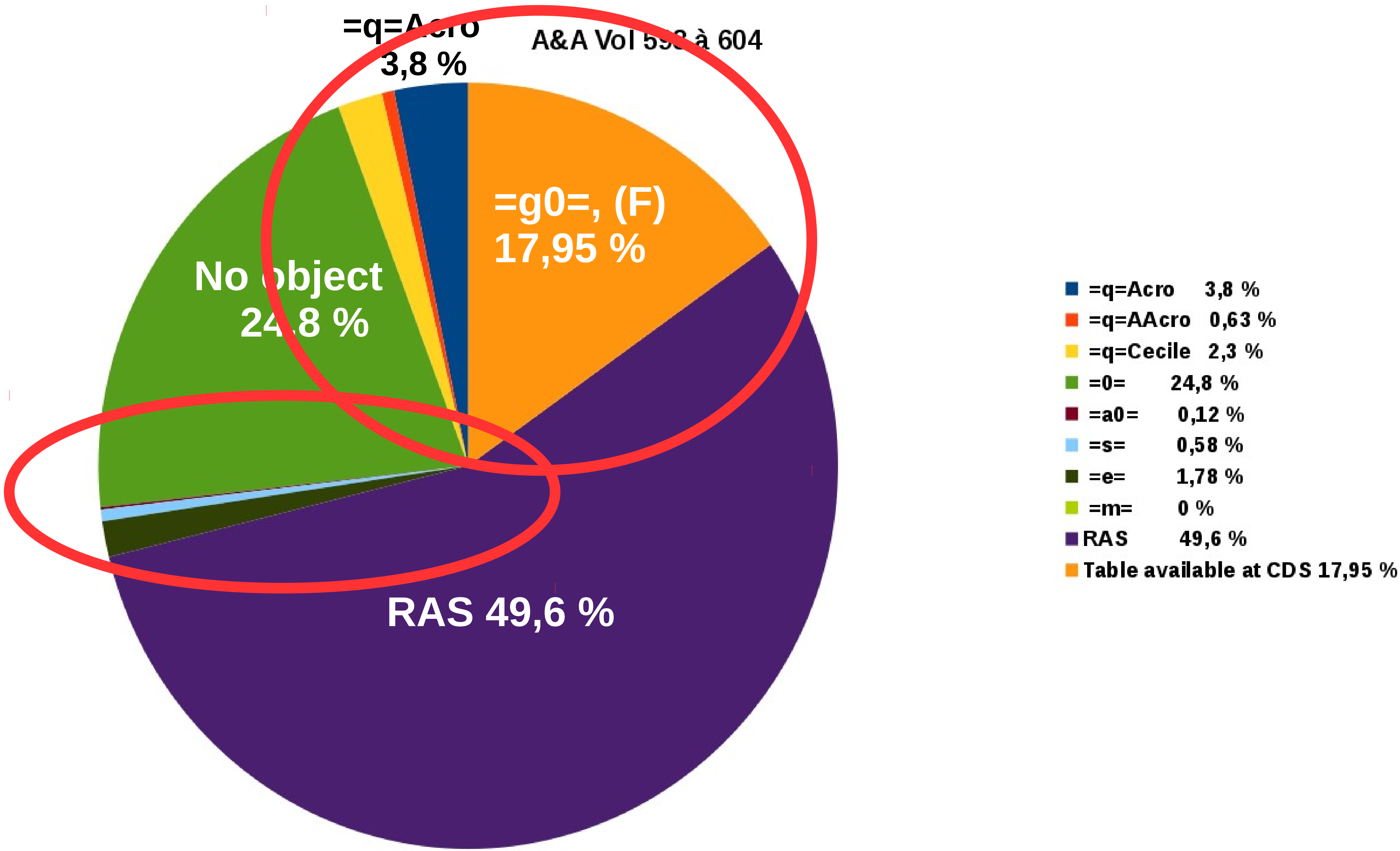

Quelques statistiques…

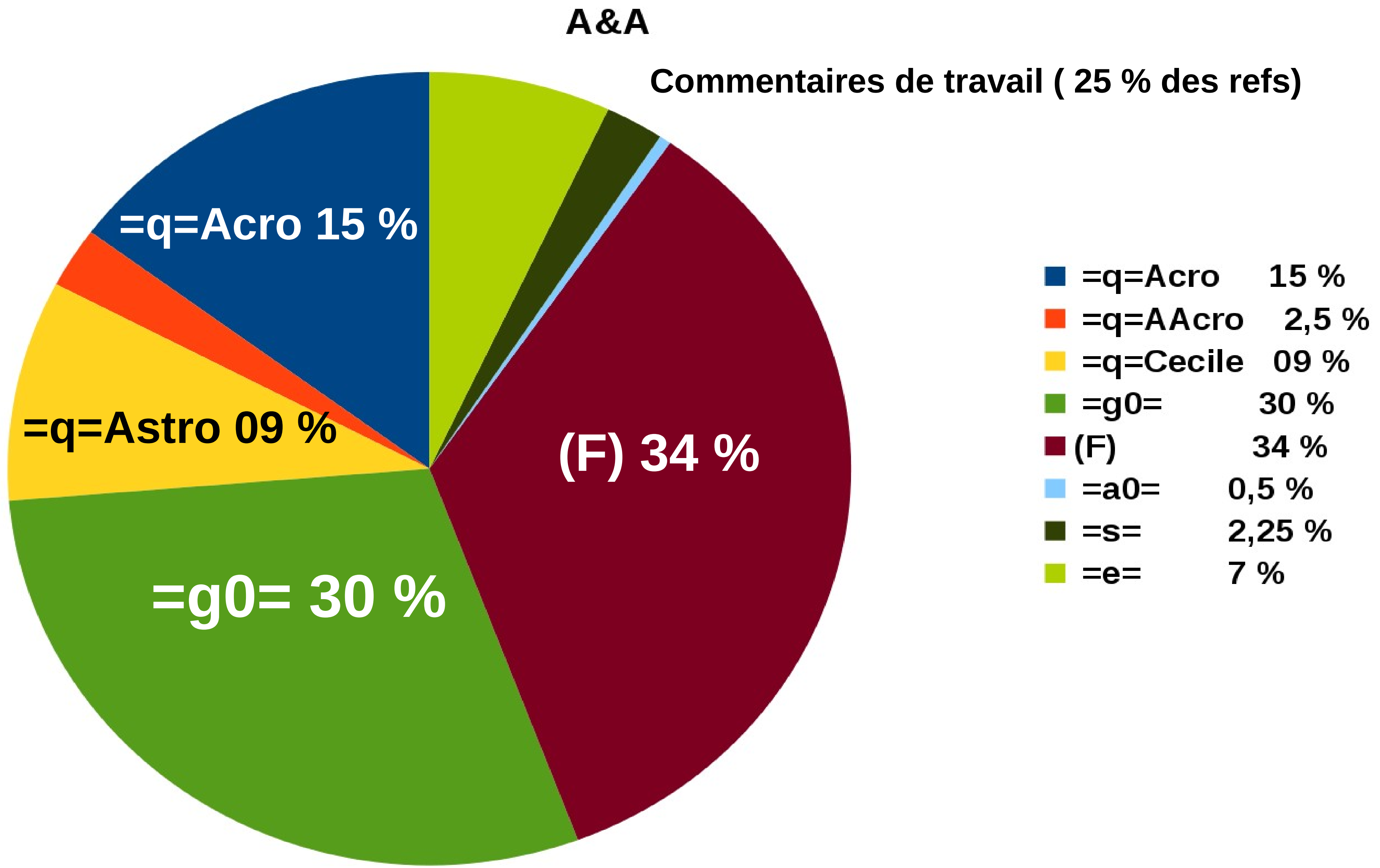

Quelques statistiques...

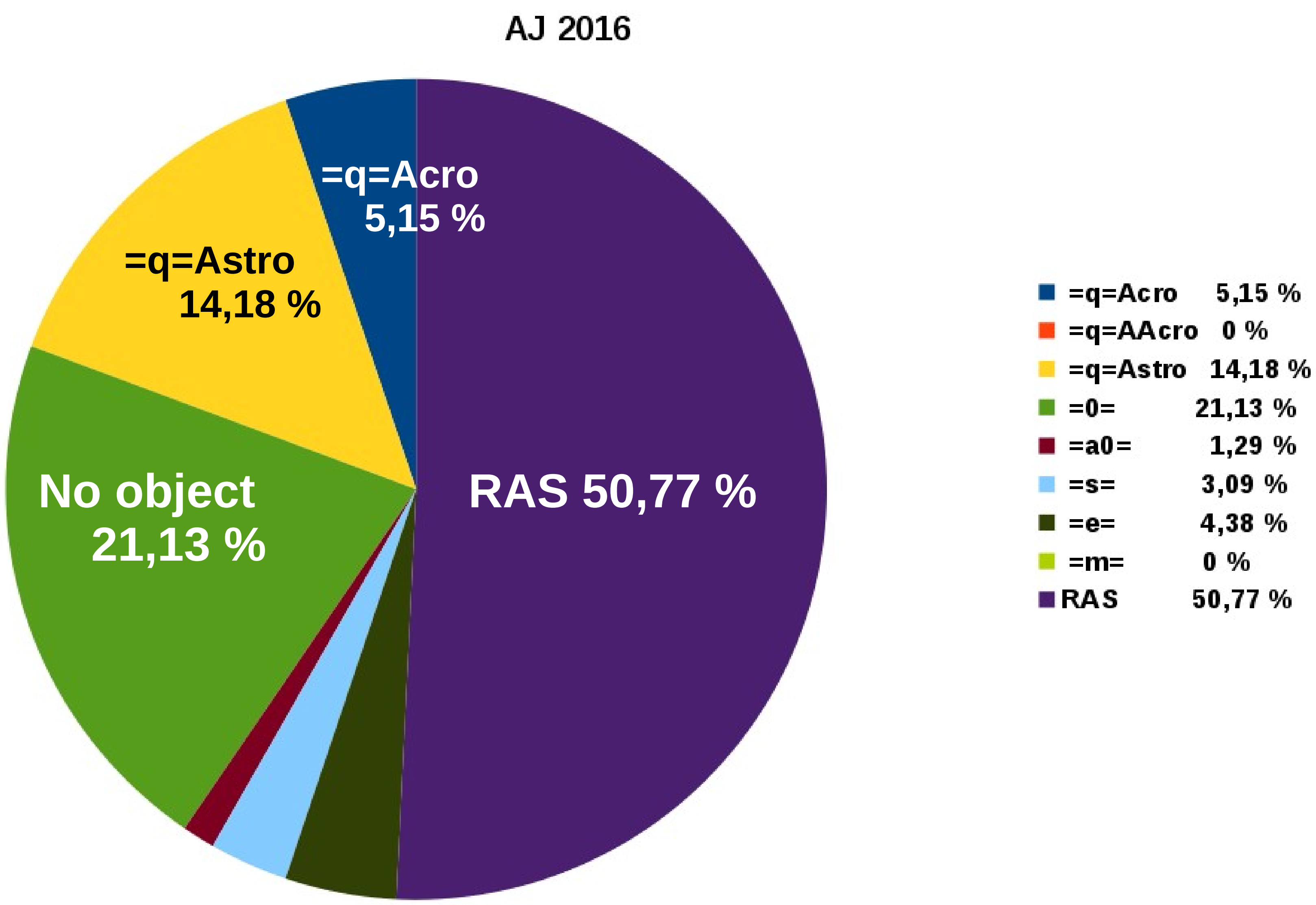

Quelques statistiques...

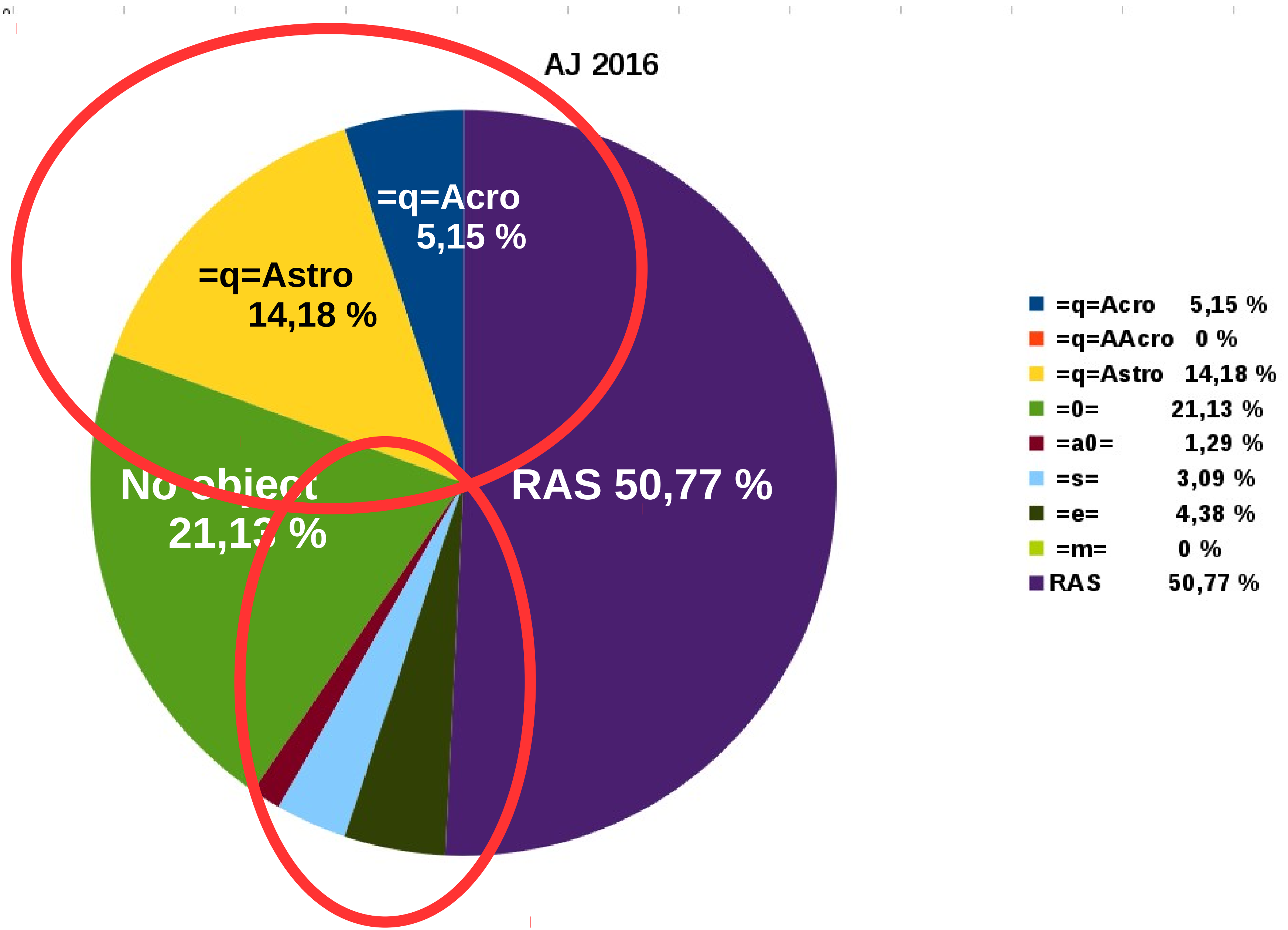

Quelques statistiques...

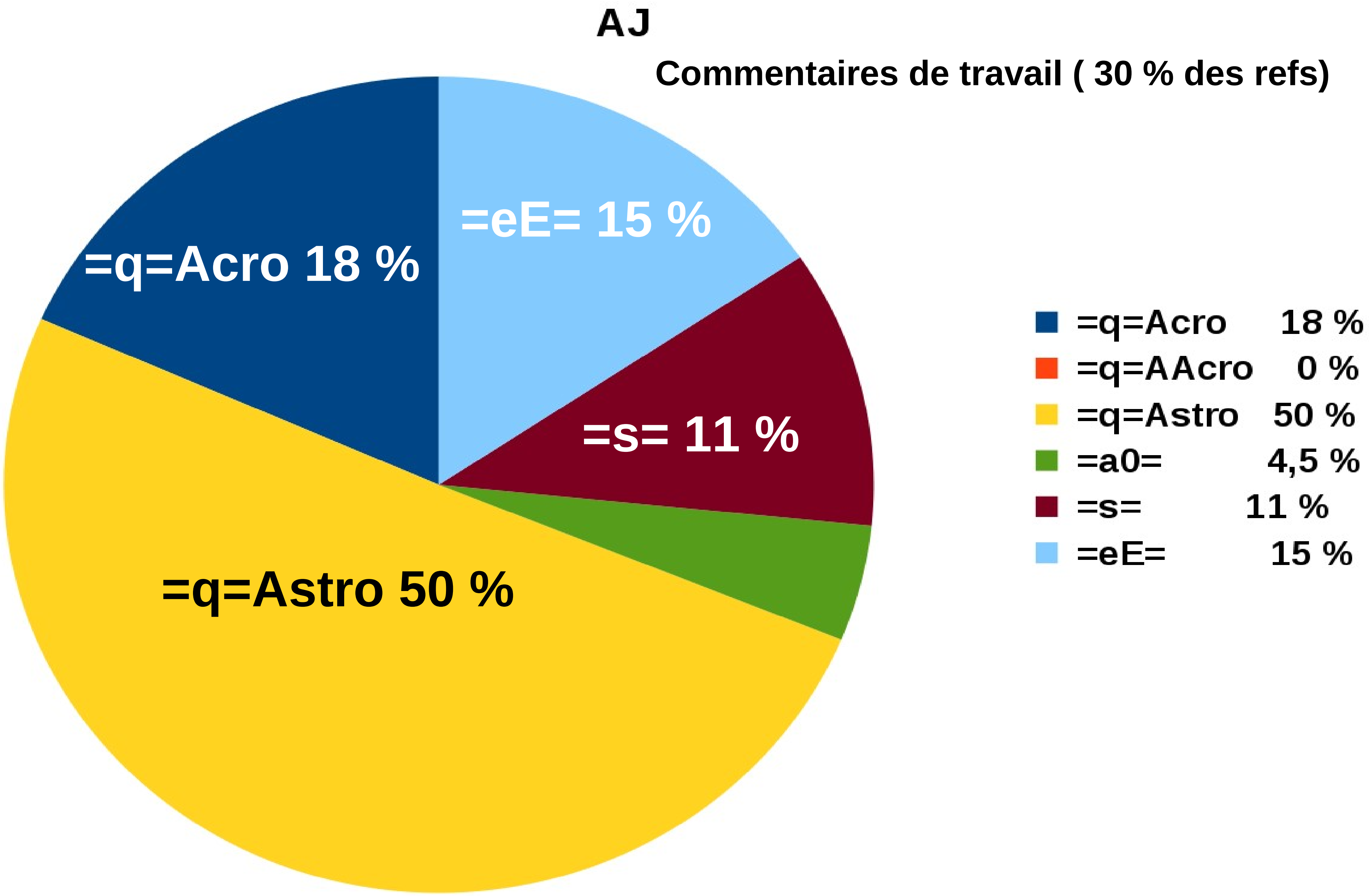

Quelques statistiques...

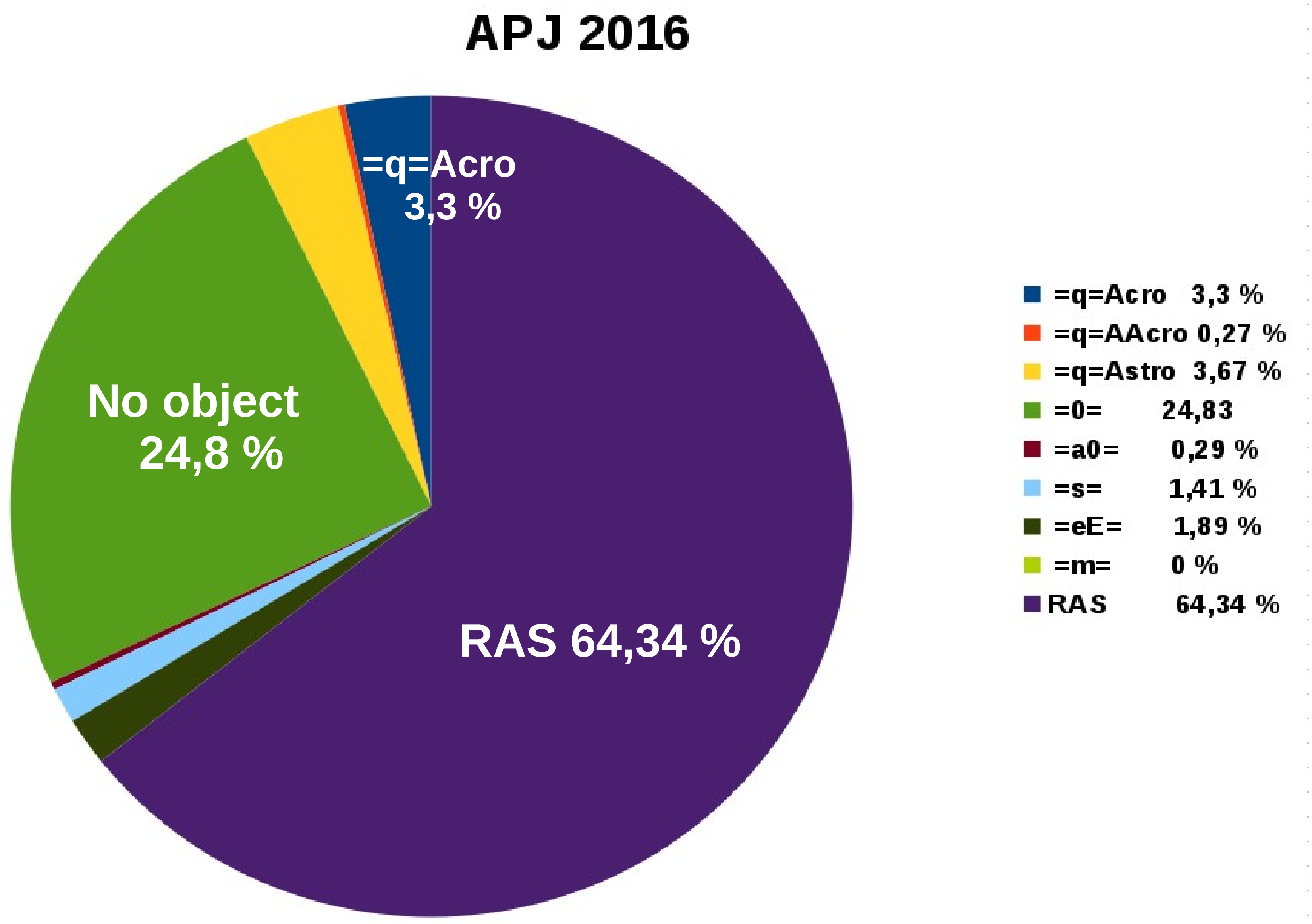

Quelques statistiques...

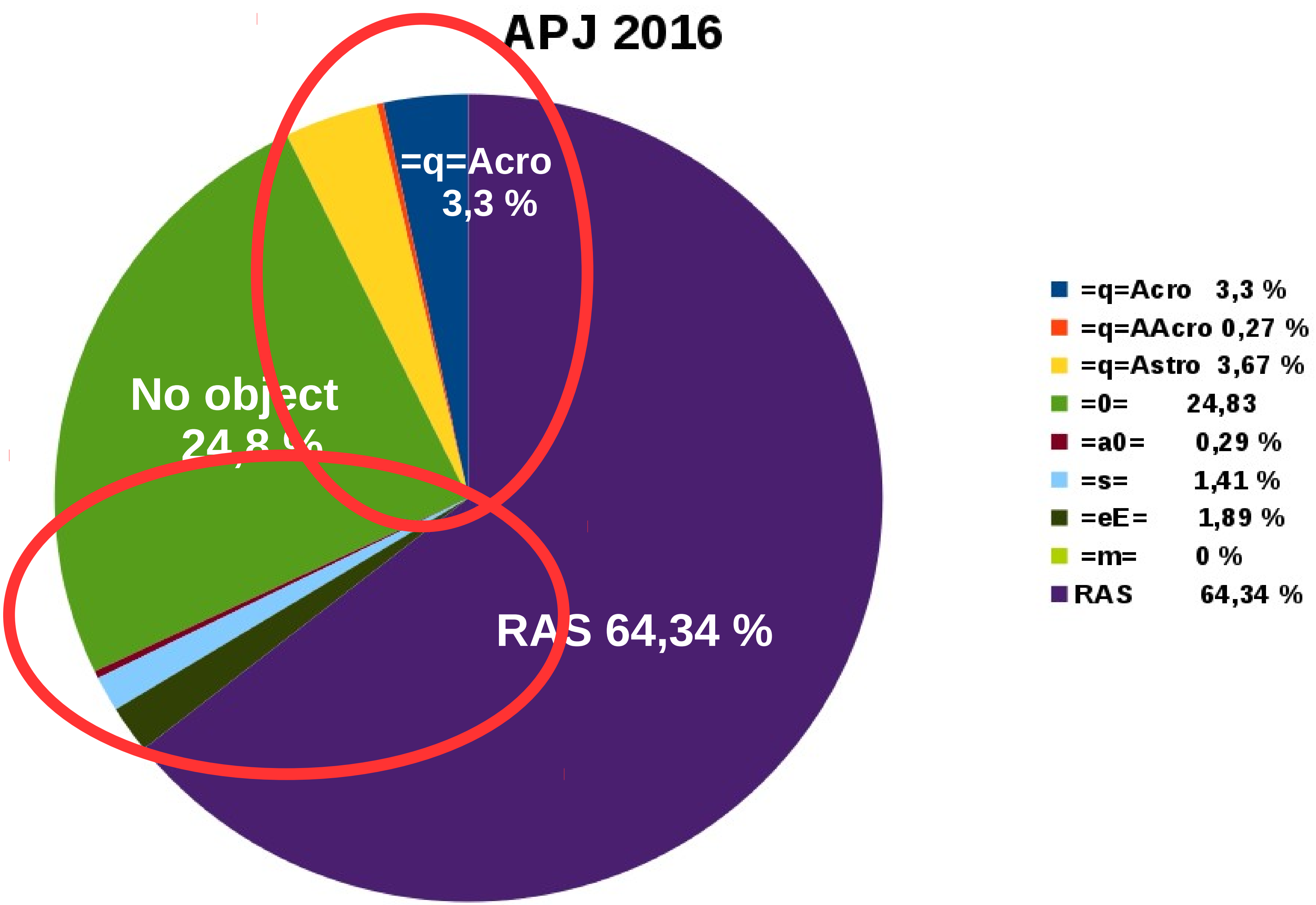

Quelques statistiques...

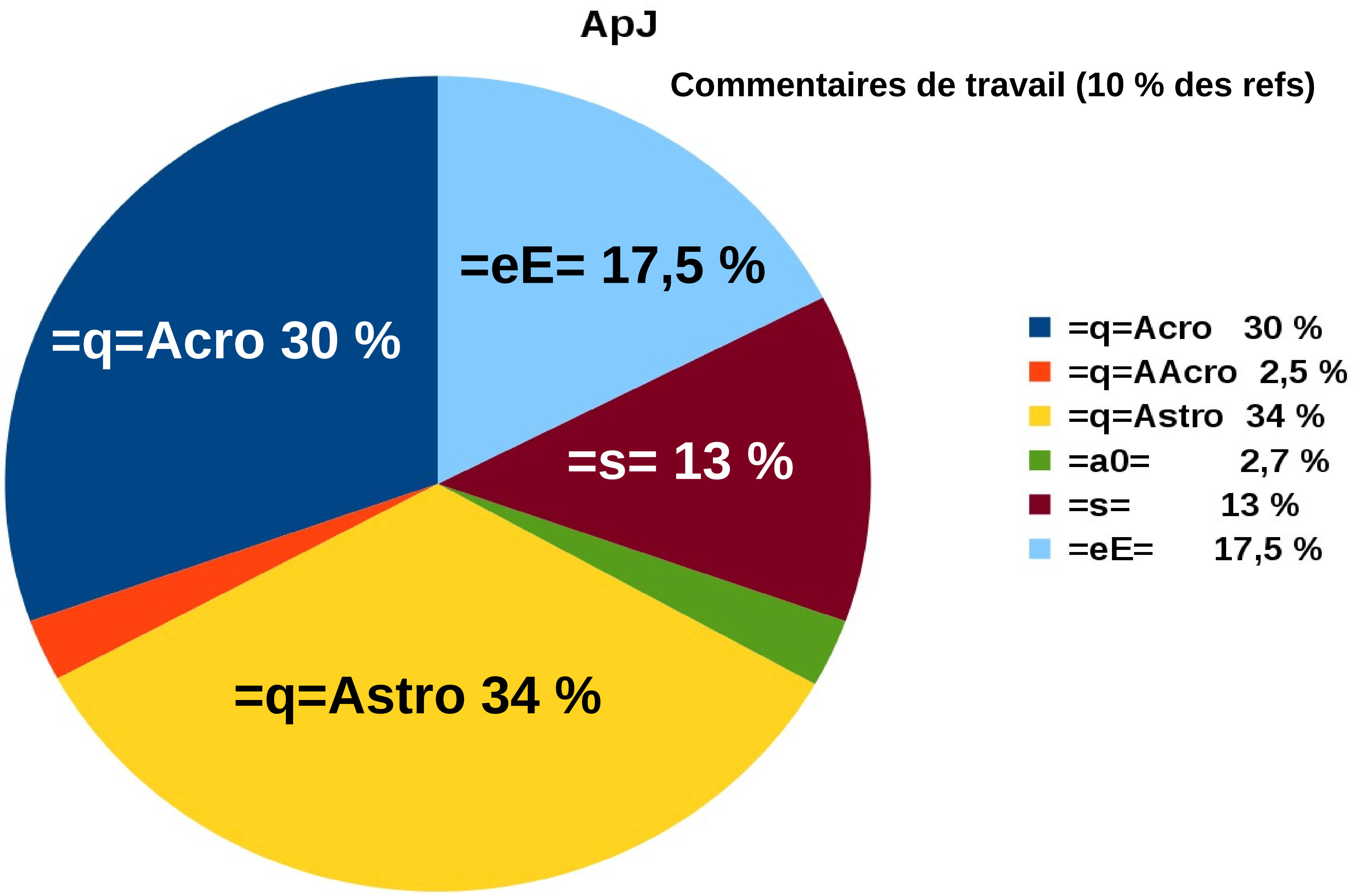

Quelques statistiques...

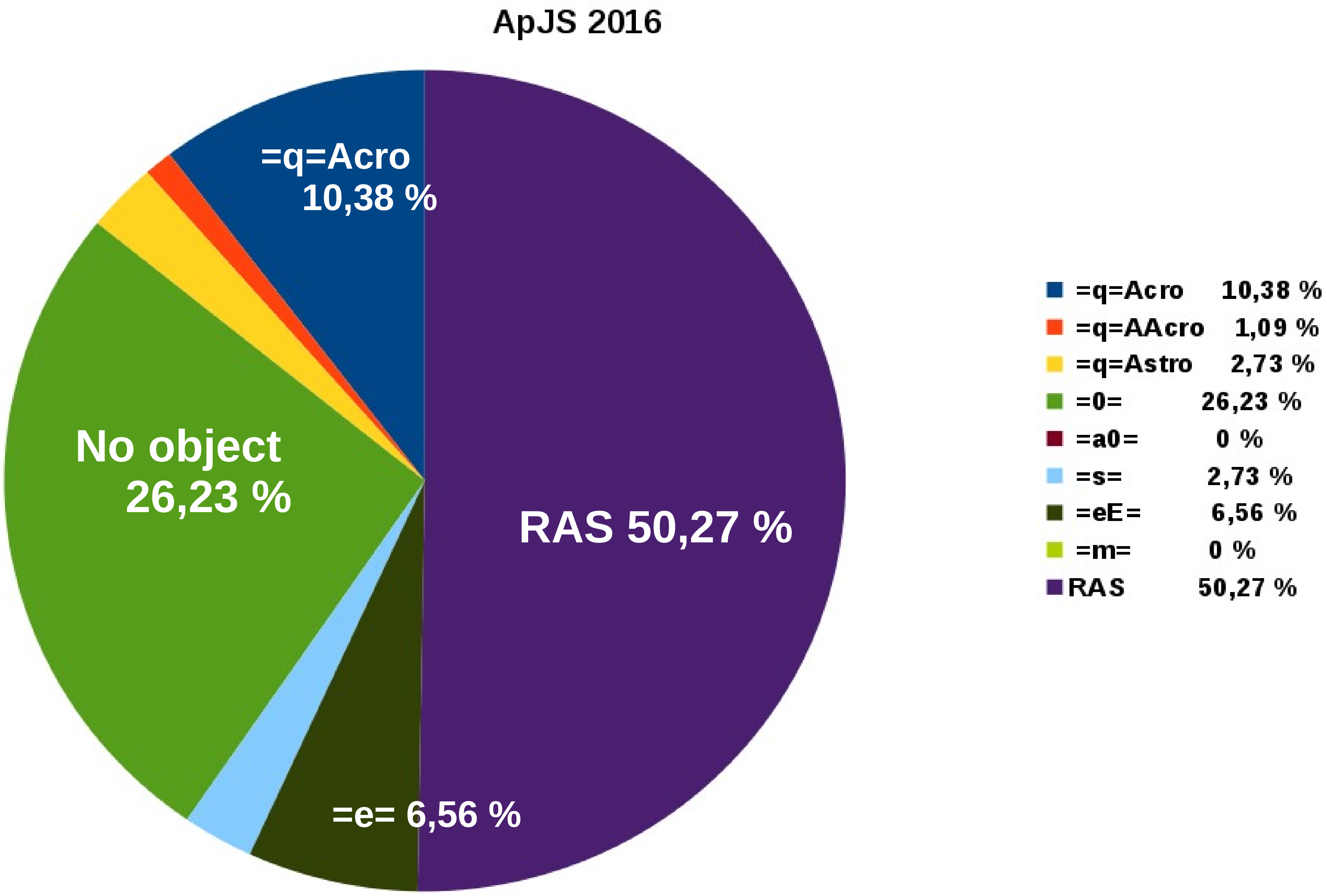

Quelques statistiques...

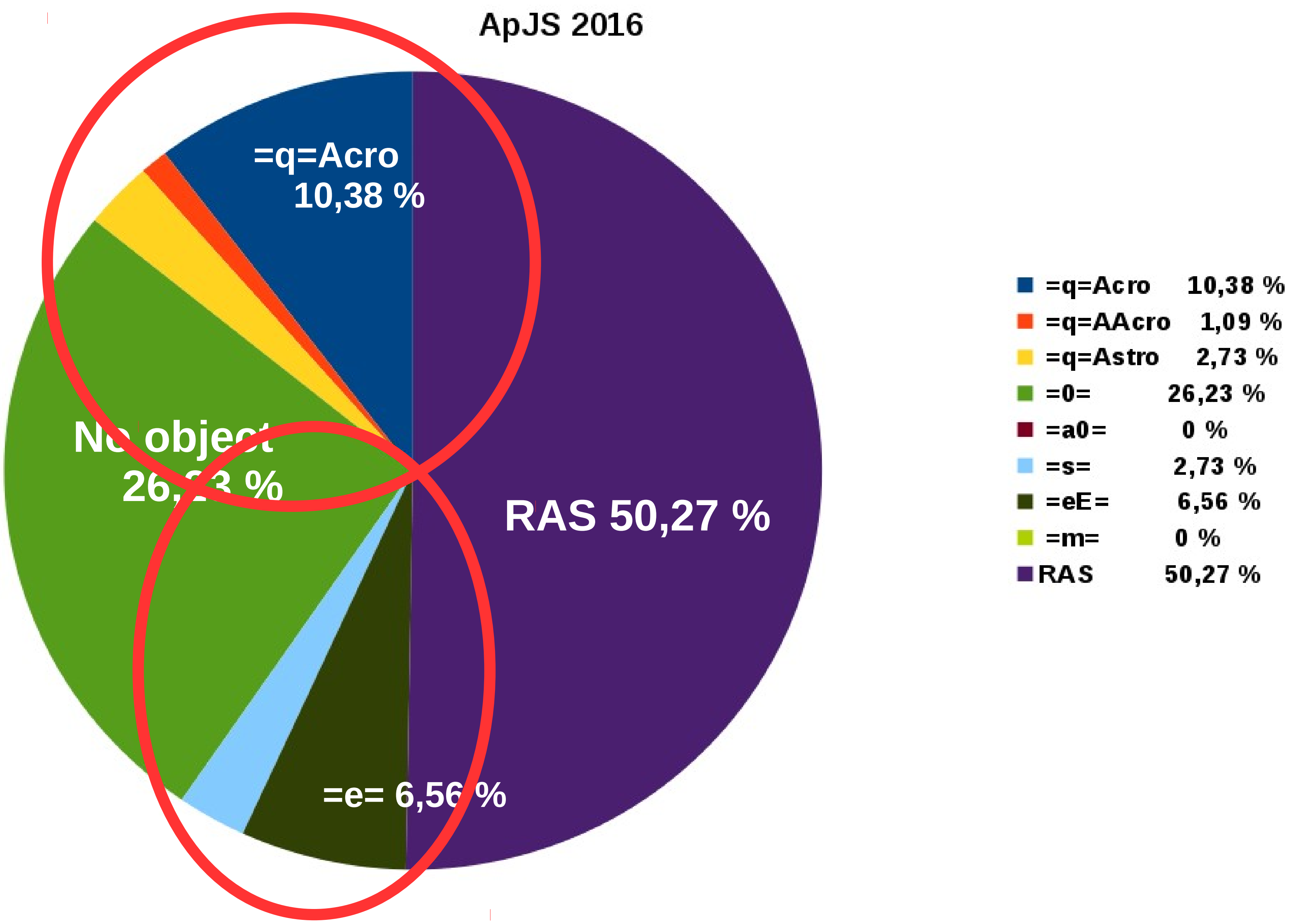

Quelques statistiques…

Commentaires de travail (25 % des refs)

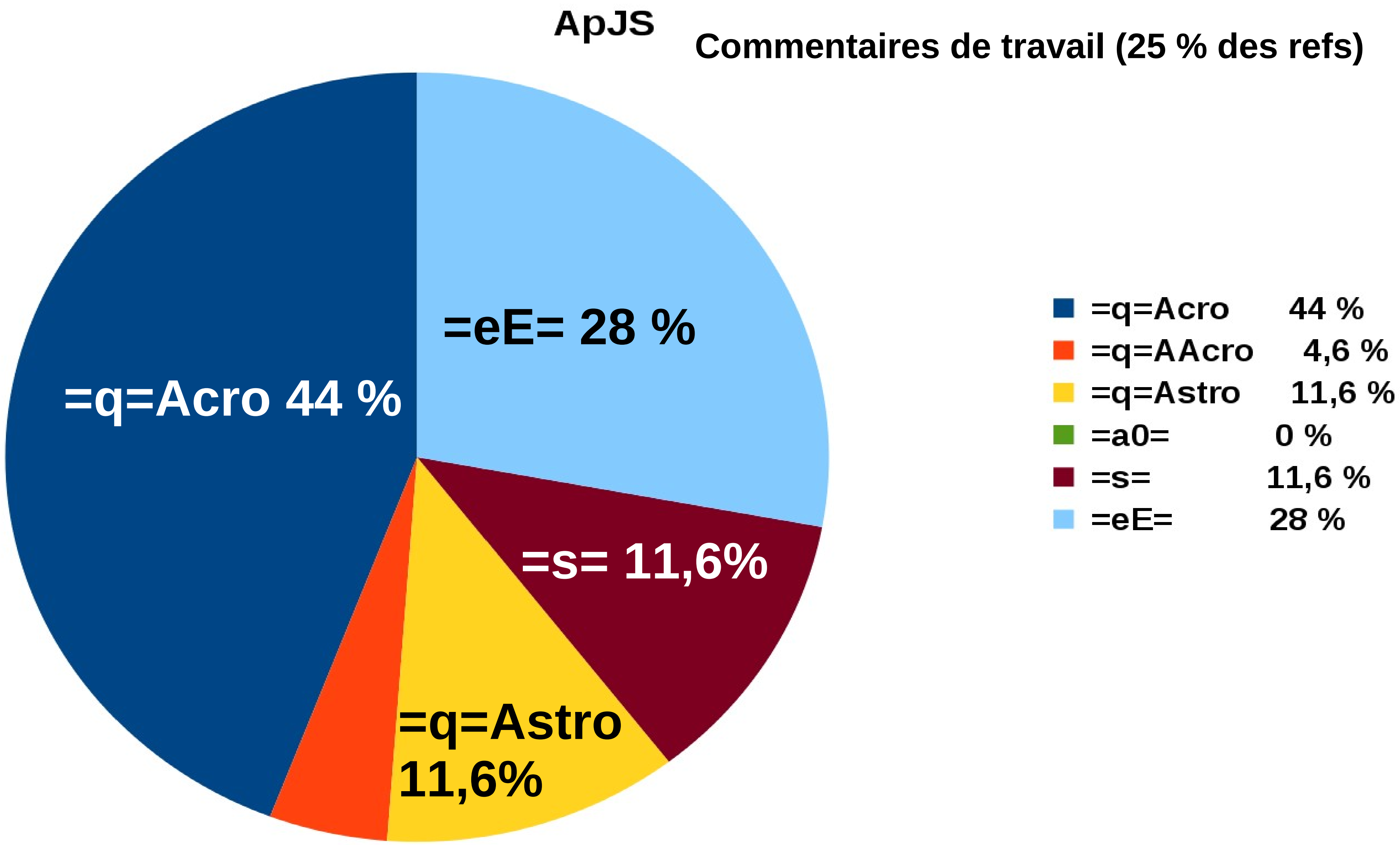

Quelques statistiques...

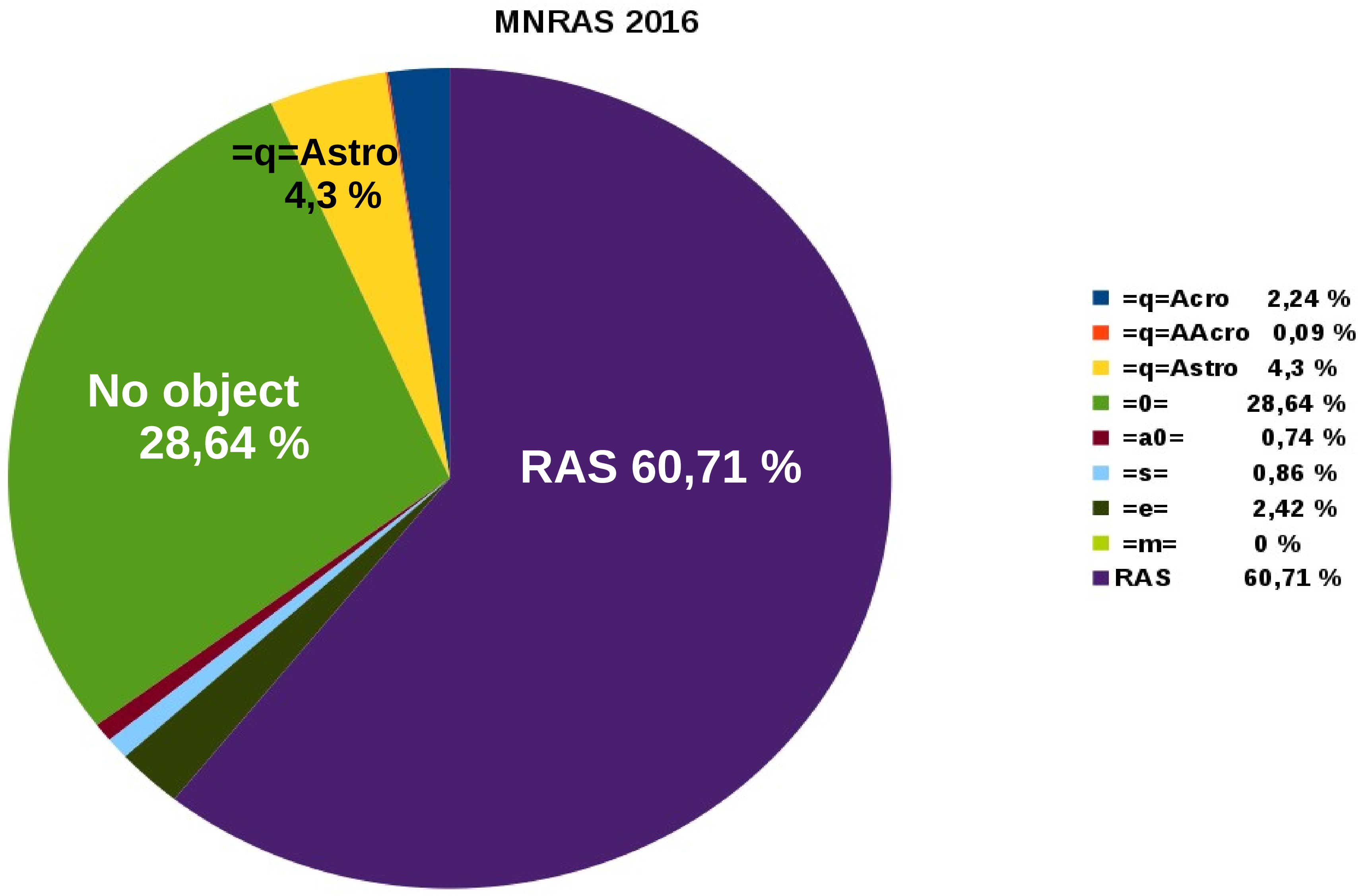

Quelques statistiques...

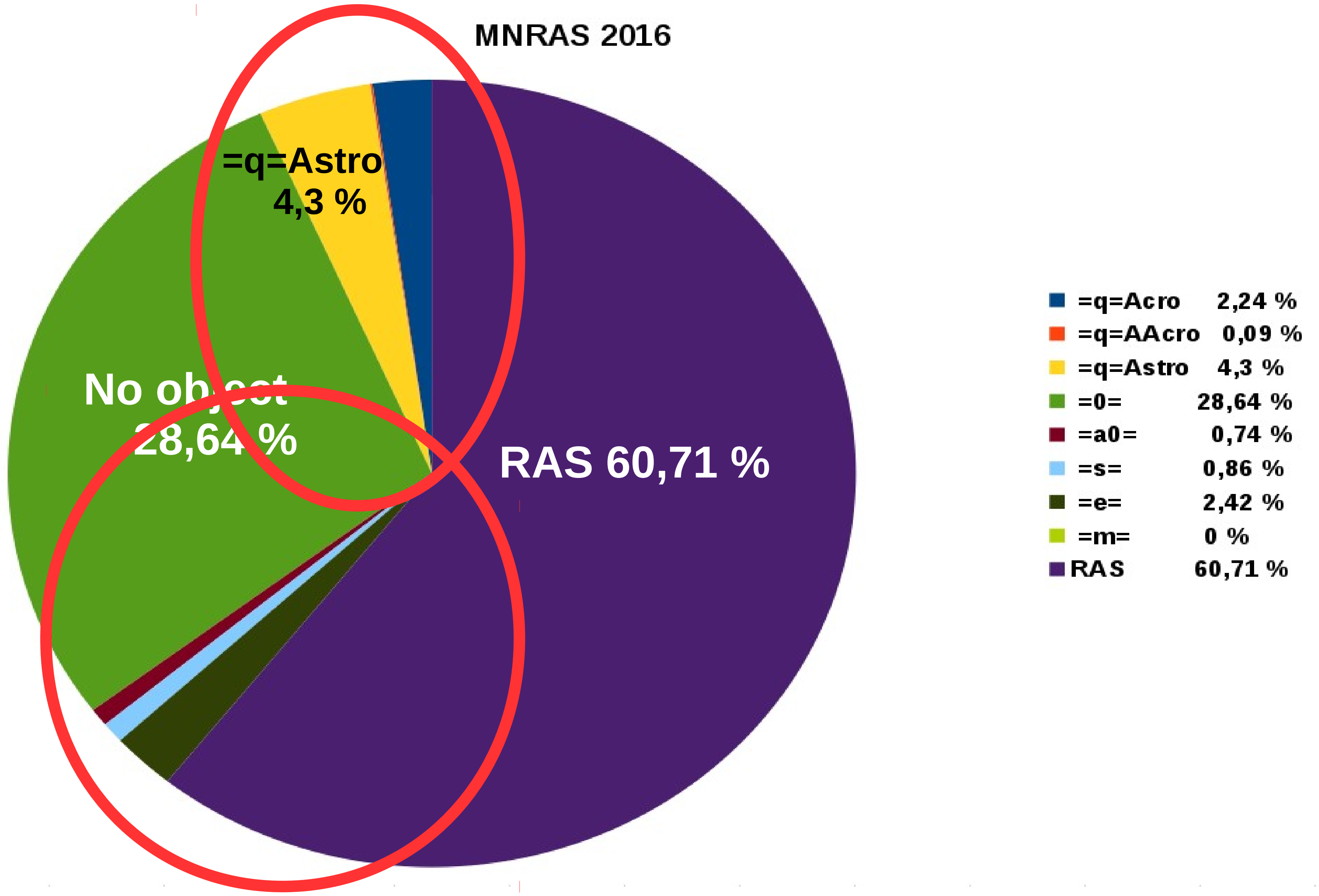

Quelques statistiques...

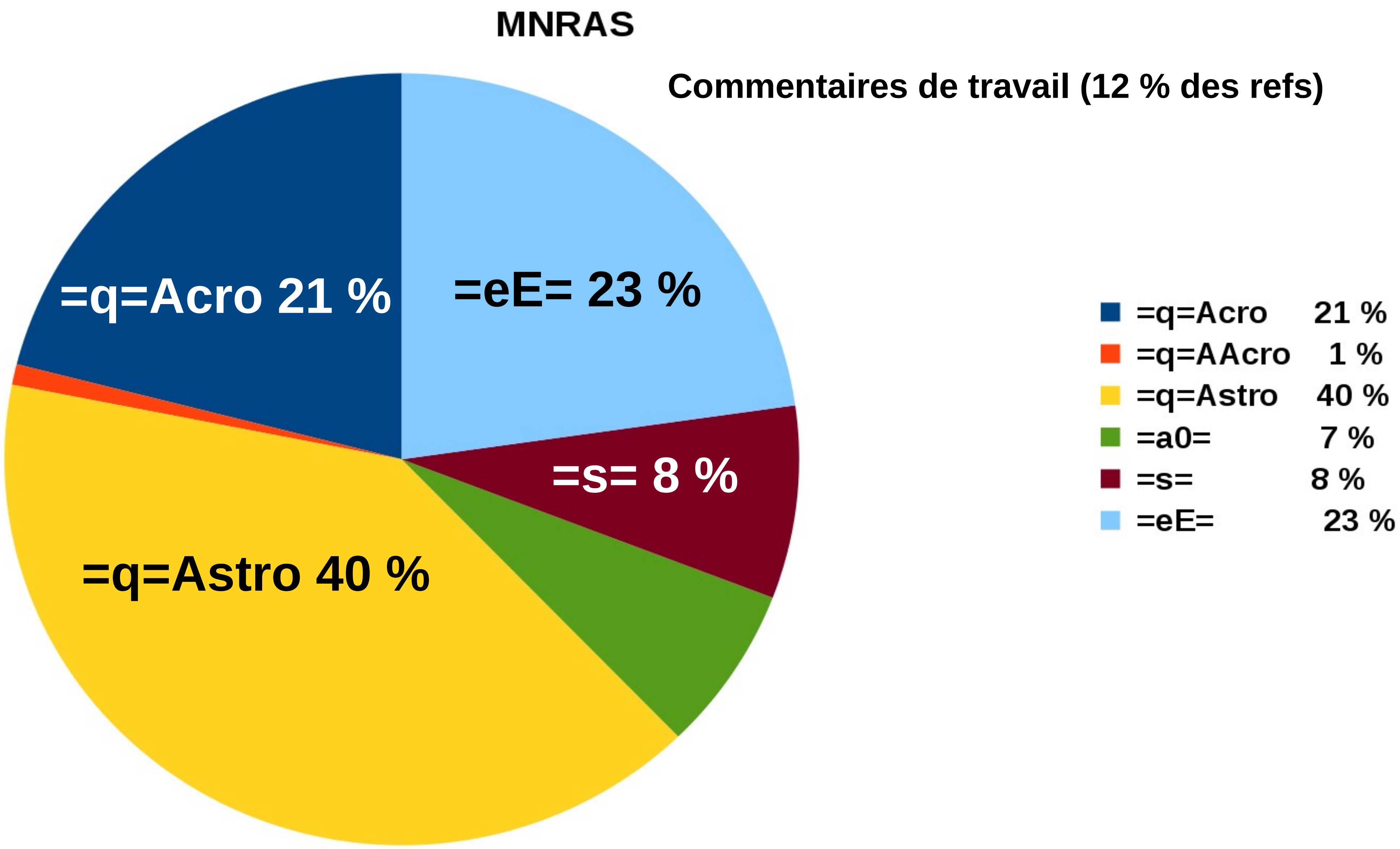

Quelques statistiques...

Détails des questions à l'astronome référent

Exemple d'Evelyne (MNRAS, AJ) sur 2 ans